Momentum exchange theory of photon diffraction

Michael J. Mobley

Momentum exchange theory of photon diffraction

Michael J. Mobley[a,b,*]
[a]Grand Canyon University, Center for Integrated Science, Engineering and Technology, Phoenix, Arizona, United States
[b]Arizona State University, The Biodesign Institute, Tempe, Arizona, United States

Abstract. Momentum exchange theory (MET) provides an alternative picture for optical diffraction based on a distribution of photon paths through momentum transfer probabilities determined at the scattering aperture. This is contrasted with classical optical wave theory that uses the Huygens–Fresnel principle and sums the phased contributions of wavelets at the point of detection. Single-slit, multiple-slit (Talbot effect), and straight-edge diffraction provide significant clues to the geometric parameters controlling momentum transfer probabilities and the relation to Fresnel zone numbers. Momentum transfer is primarily dependent on preferred momentum states at the aperture and the specific location and distance for momentum exchange. Diffraction by an opaque disc provides insight to negative (attractive) dispersions. MET should simplify the analysis of a broadened set of aperture configurations and experimental conditions. © *The Authors. Published by SPIE under a Creative Commons Attribution 3.0 Unported License. Distribution or reproduction of this work in whole or in part requires full attribution of the original publication, including its DOI.* [DOI: 10.1117/1.OE.57.1.015105]

1 Introductionm

"It seems to be a characteristic of the human mind that familiar concepts are abandoned only with the greatest reluctance, especially when a concrete picture of phenomena has to be sacrificed."

Max Born and Emil Wolf[1]

Momentum exchange theory (MET) is presented as an alternative picture for photon diffraction based upon quantized momentum transfer with the scattering lattice or aperture.[2–6] MET draws from the early ideas of Duane[7] and later formalized by Landé.[8–11] MET starts from a momentum representation for scattered particles and postulates the probability distribution for diffraction scattering is determined by at least two important factors: (1) the momentum transfer states of the scattering lattice and (2) the distance over which momentum is transferred between the lattice and scattered particle. The distinct feature of MET is this dependence on the specific path of the scattered particle and location of momentum transfer. Classical optical wave (COW) theory leaves us with an erroneous understanding of diffraction in suggesting that the probability for detecting a diffracted photon is determined on observation at the point of detection.[2,5] This picture is conceptually flawed as the probability must be determined at the location of scattering to conform to conservation of momentum. The current paper compares and contrasts MET with optical wave theories to elucidate these underlying momentum exchange selection rules. This picture is important as it illuminates our debates over the wave-particle nature of light and quantum uncertainty, framing the contrasts between the standard (Copenhagen) interpretation and several alternative interpretations.[12–16]

For clarity, it is important to emphasize here the distinction between diffraction, which relates to the scattering and probability distribution for individual photons, and interference, which is a cooperative phenomenon that relates to the probabilities of detection (absorption?) when there is a multiplicity of photons (e.g., two electromagnetic beams) that can influence each other at the point of detection. An individual particle cannot interfere with itself. Detection of a photon is dependent on its polarization and phase (orientation?) and the polarizability of the electronic states of a detector (antenna or molecule) it interacts with. Thus, based upon the characteristics of detection, multiple photons, concurrently at a detector, can affect the potential for each to be absorbed (can interfere). Observed optical phenomena can involve diffraction, or interference, or both (e.g., laser holography).

In the 1920s, Duane[7] and later Ehrenfest and Epstein[17] showed diffraction could be explained in terms of a momentum change by interaction with a scattering lattice dependent on the geometry and momentum states of the lattice that can be analyzed according to Fourier's theorem. These early ideas seemed to be lost with the initial formulations of wave mechanics, but were later revived by Landé, who used them in his formulation of quantum theory.[8–11] The primary learning from these formulations is that the probability distribution for the scattering of a particle is determined by the geometry of the scattering lattice, much as the angular distribution of light diffracted in classical optical theory is the Fourier transform of the aperture or obstacle.[18,19] These ideas languished because of the success of classical electrodynamics and wave mechanics to explain both optical diffraction and interference, despite their conceptual challenges. More recently, Van Vliet[20] refreshed these early ideas of Duane and Landé with an updated treatment of diffraction by linear momentum quantization through periodic structures, again stressing this approach avoids a dual nature to quantum particles. Momentum conservation is preserved without retardation. An additional contribution of this work was

*Address all correspondence to: Michael J. Mobley, E-mail: Mike. Mobley@gcu. edu

the examination of systems with reduced symmetries. Such descriptions are more consistent with later formulations of quantum theory, such as the statistical interpretation of Ballentine[21] or path integral approach of Feynman.[22]

Storey et al.[23] joined this debate on interpretations examining a familiar "welcher Weg" (which way) experiment associated with double-slit diffraction, describing the photon scattering in terms of a momentum representation and quantized momentum transfer. The observation was again put forward that the interference pattern was determined by the uncertainty principle. Here, it was described that a microwave radiation exchange within the diffracting aperture is responsible for a transverse momentum "kick" to the scattered photon. Wiseman et al[24] provide further perspective describing a formalism to analyze momentum transfer in welcher Weg double-slit diffraction experiments using the Wigner function. This question was also analyzed using Bohm's formulation of quantum mechanics in which scattered particles have a definite position and momentum at all times.[25] This approach conceptualizes the interaction and momentum exchange at the diffracting slits and suggests the potential application of Bohmian trajectories to single-slit and other diffraction configurations. This treatment demonstrated the utility of defined particle paths and opens the possibility that this formalism can accommodate geometrically defined transfer functions that are dependent on the separation of the path from the aperture boundary proposed by MET.

The argument for the MET picture will be built in succeeding sections. Section 2 provides a contrast and comparison of optical wave theories with MET noting a common connection in the Fourier transform. Section 3 examines a momentum representation of the equations of classical optical theory to point out their dependence on momentum exchange at the scattering aperture. Section 4 reviews single-slit diffraction, demonstrating that scattering probabilities are dependent on momentum state functions of the slit and suggesting that the scattering will be dependent on the path of the photons. Section 5 provides a similar analysis of straight-edge diffraction connecting momentum exchange probabilities to the analysis of Fresnel zones. Section 6 provides an analysis, working backward from the straight-edge diffraction pattern observed, to define the probability distribution for momentum exchange with photons in the plane of the straight edge. This analysis demonstrates the dependence of the scattering on the path of the photon. Section 7 extends the analysis to multiple slits and the Talbot effect. Section 8 reviews diffraction by a circular disc to examine negative (attractive) momentum dispersion of photons in the plane of the disc. Section 9 generalizes the MET formalism for broader application. Section 10 looks at the implications and predictions for other experimental configurations.

2 Contrasting Pictures of Diffraction

To aid our understanding of this more integrated picture, we contrast MET with the predominant historical pictures that have emerged for diffraction phenomena.

2.1 *Picture 1: Classical Optical Wave Theory*

COW was built on the Huygens–Fresnel principle that assumes a spherical dispersion of the light as wavelets in the vicinity of the aperture with phase summation and interference determining the light intensity at detection. COW has been very successful in describing the diffraction of light.[26,27] Physicists have translated optical wave theory into the mathematical formalism of quantum mechanics that better reflects the statistical foundations of QM (see Ref. 28). This established a common theoretical foundation for the diffraction of photons, electrons, and other fundamental particles based upon the interference for a particle wave. However, this wave picture is misleading as it implies a broad extension of a photon wave and that the probability for a photon path is determined at the point of detection. The formalism identifies the intensity at a detection point but maintains an uncertainty in the momentum vector. There remains a significant gap between the conceptual foundations of wave theory and the descriptions of particle scattering we obtained from both classical mechanics and the more recent formulations of quantum theory that invoke quantized momentum exchange, such as quantum electrodynamics (QED).[29]

2.2 *Picture 2: Boundary Diffraction Wave Theory*

This alternative description of optical diffraction [boundary diffraction wave (BDW)] assumes that the observed intensity consists of a superposition of the incident wave transmitted unperturbed and a diffraction wave or boundary wave originating at the rim of the aperture. Though less known, this is viewed to be more "physical" than the standard Huygens–Fresnel principle and was first qualitatively expressed by Thomas Young in 1802.[19] A rigorous solution to the straight-edge/half-screen problem was described by Sommerfeld.[30] Miyamoto and Wolf[31,32] generalized the theory of a BDW offered by Maggi-Rubinowicz. A closely related approach is the geometrical theory developed by Keller,[33] replacing the superposition of incident and diffraction waves with the principles of geometric optics. This is similar to Huygens–Fresnel in that the fields associated with the incident, reflected, and diffracted rays are superimposed to define a field amplitude and probability at the point of detection. Kumar et al.[34] demonstrated the utility of this theoretical approach in describing experimental knife-edge diffraction while also confirming compatibility with COW. An important conceptual contribution of this picture is the direct connection between the aperture and the scattered wave. However, Kumar[35] pointed to an insufficiency to this approach in that the phase shift required for the diffraction wave would point to a discontinuity at the geometric shadow that is not confirmed, suggesting we expand our thinking on the nature of diffraction. More recently, Umul[36] has connected the surface integrals of physical optics, separable into two subintegrals, with the potential functions of BDW theory.

2.3 *Picture 3: Momentum Exchange Theory*

The interfering wavelets of COW and BDW suggest that the probability for detecting a diffracted photon is determined on observation at the point of detection. I have argued these pictures are both conceptually flawed as the probability must be determined at the location of scattering to preserve conservation of momentum. MET draws from a momentum representation and postulates the probability distribution is determined by the particle path, experimental geometry, and momentum transfer states at the scattering aperture. Earlier

formulations[7–10] suggested that the experimentally observed boundaries for momentum transfer, Δp, are a multiple of Planck's constant, h, over a periodic dimension, L, such that $\Delta p = nh/L$, or, frequently experimentally observed

$$\Delta p_x = \frac{jh}{2L}, \tag{1}$$

where n and j are integers. Diffraction can be described in terms of a diffraction force, characterized by momentum exchange defined by geometric properties of the scattering structure. The insight emphasized in this paper is that the momentum exchange associated with diffraction is also a specific function of the distance of exchange.

2.4 Geometric Correlations of Theories

The distinctions and similarities between these three different pictures of diffraction are illustrated in Fig. 1, which was detailed in an earlier paper.[5] The diagrams depict the diffraction of monochromatic light with a detection point at P and a reference point for diffraction at O. We assume the x, y plane is normal to the propagation vector of the light that aligns with the segment $\overline{AP}$. Our plane of interest contains
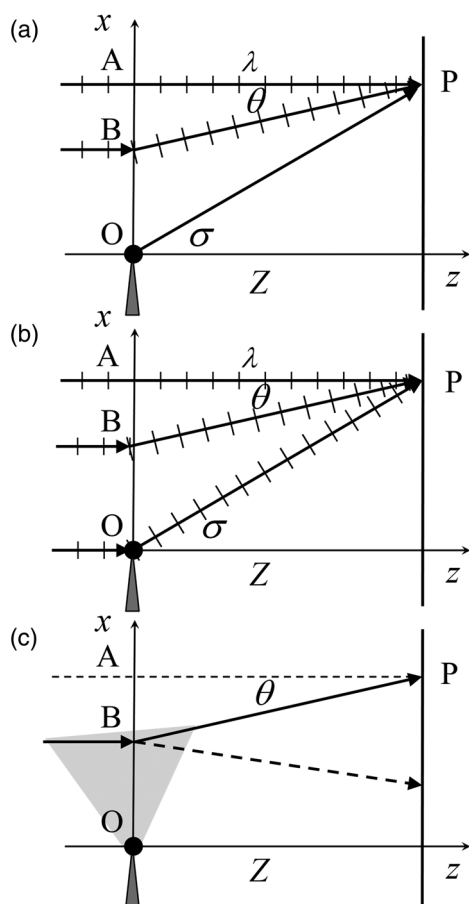
Fig. 1 Three different conceptual pictures for optical diffraction related to a reference point at O with light intensity measured at P. (a) COW picture based upon the Huygens–Fresnel principle summing the interference between wavelets emanating in the x, y plane; (b) the BDW theory picture with $\overline{OP}$ representing the diffraction wave; and (c) the MET picture with the scattering of photons by quantized momentum exchange determined by the proximity of the scattering boundary point.

the propagation vector (light ray) from the source to point P and the reference point, O. Figure 1(a) illustrates the Huygens–Fresnel principle of COW, where Huygens wavelets are generated in the x, y plane. The segment $\overline{BP}$ depicts the path of one wavelet that can be compared with the path and phase of $\overrightarrow{AP}$. In COW, the diffraction field intensity is calculated via the weighted sum (integral) of all the Huygens wavelet paths that converge on the detection point, P. The intensity calculation is derived from the relative phase contribution of each wavelet, dependent on the relative lengths of the segments, e.g., $\overline{AP}$ and $\overline{BP}$. As the lengths of two sides and one angle of a triangle always determine the length of the third side, the lengths of $\overline{AP}$ and $\overline{BP}$ uniquely determine $\overline{AB}$. Similarly, $\overline{OP}$ and $\overline{AP}$ will determine $\overline{OA}$ and thus, $\overline{OB}$ is also defined. To clarify, this phase difference, $\Delta\text{phase} = -i2\pi\Lambda/\lambda$, between any unperturbed (reference) wavelet of length, $\overline{AP}$, and any dispersed wavelet of length $\overrightarrow{BP}$ is a function of the difference in the lengths, $\Lambda = \overline{BP} - \overline{AP}$. As $\overline{BP} = \overline{BA}/\sin\theta$ and $\overline{AP} = \overline{BA}/\tan\theta$, the phase variation for a Huygens wavelet at a detection point will always depend on the angle of deflection and a reference distance along the x or normal axis

$$\Lambda = \frac{\overline{BA}(1 - \cos\theta)}{\sin\theta}. \tag{2}$$

Assuming the Fraunhofer region of diffraction and using the small angle approximation

$$\Lambda \cong \overline{BA}\,\sin(\theta/2) \cong \frac{\overline{BA}}{2}\,\sin\theta. \tag{3}$$

This parallels the Fourier transform dependence on the transverse dimensions in this formalism; recognizing the Fourier transform directly connects an aperture function to a far-field function.[37] Two wavelet trajectories can be related through the relation of each to the phase of a reference wavelet. I emphasize that these geometric relations are axiomatic and not the result of alternative theoretical considerations. There is a fundamental connection between an angle of deflection and the "phase separation."

Figure 1(b) illustrates BDW theory, where $\overrightarrow{OP}$ represents the ray associated with the diffraction wave scattered from our reference point, O, that might be associated with the edge of an aperture. $\overrightarrow{AP}$ is the path of the unperturbed ray and $\overrightarrow{BP}$ is the path of a perturbed ray. This approach sums the phases of all the rays reaching the detection point, P. From the geometry of this depiction, we can assert that the phases at the detection point will be dependent on the distances, $\overline{OA}$ and $\overline{OB}$, and the deflection angle.

As the relation of Eq. (3) is axiomatic, the scattering probability distribution derived via the Huygens–Fresnel principle can always be reframed in terms of momentum exchange probabilities determined by geometries of the scattering lattice. I will demonstrate that by adopting a momentum representation for the mathematical formalism used in COW and BDW, we can develop a connection to these probabilities and intensity profiles that our geometric analysis demonstrates must exist. Familiar tools to make this connection will be the Fresnel zones and the Fresnel number that can be related to momentum exchange. Figure 1(c) illustrates MET, where photons passing the reference point O near B are scattered by

the exchange of momentum and deflected to P, with the probability being dependent on the selection rules for momentum exchange. To clarify, in the momentum representation, where the photon momentum is $p = h/\lambda = \hbar k$, the rotation of the photon trajectory in the x, z plane, θ, is connected to a change in momentum along the perpendicular (x) axis, $\Delta p_x = p \sin \theta$, and the momentum change (reduction) along the z-axis, $\Delta p_z = p(1 - \cos \theta)$. Thus, the relative phase variation will depend on as follows

$$\Delta \text{phase} = \frac{-2\pi\Lambda}{\lambda} \cong \frac{-\pi\overline{\text{BA}}\Delta p_x}{h} \cong \frac{-\pi\overline{\text{BA}}}{\lambda_e} \cong \frac{-\overline{\text{BA}}}{2}\text{k}_e, \quad (4)$$

where λ_e used here is associated with an effective wavelength defining momentum exchange and the phase change is related to the ratio, $\overline{\text{BA}}/\lambda_e$. With this conversion, our probabilities for momentum exchange must involve a geometric summation (integral) at the aperture that parallels the summation of phases we determine in the far field. This will be the approach developed further in the next sections of this paper. We will note an advantage to this approach is that probabilities can be associated with individual light paths that simplify the analysis of a broadened set of aperture configurations and experimental conditions. The approach also provides insight to the phase problem or the Fresnel phase-shift that is associated with the classical or Fourier representation of diffraction.

3 Mathematical Foundations for Photon Diffraction

An excellent visualization of slit diffraction of photons was provided by Harris et al.,[26] who compared the experimental results from high-resolution diffraction patterns with the theoretical predictions of optical wave theory in the Fraunhofer and Fresnel regions and found an excellent agreement between the calculated and observed patterns. This work produced plots of the scattering patterns at different distances from the slit that provide an indication of how the light scattering pattern near the slit progressively fans out as a detector screen moves farther from the diffracting slit. From this, we can visualize the distribution of paths followed by scattered photons. We can use the COW formalism to relate to a description of photon diffraction in terms of quantized momentum transfer. Adopting this approach does not endorse the wave picture that classical optical theory presents, but rather it is used to demonstrate the axiomatic compatibility with our MET formulation for particles. I will start with a generalized description of light diffraction based on the Rayleigh–Sommerfeld and the Fresnel–Kirchoff theories of diffraction. I consider diffraction of light by an aperture in the x, y plane at $z = 0$. I assume a light source treated as a monochromatic plane wave initially propagating along the z-axis. This can be experimentally modeled with laser light. An additional assumption is that the source of light is sufficiently dilute that the response of any detector used is linear to the intensity of light—to the number of photons reaching the detector. This also assumes that there is no co-operative phenomenon (interference) observed at the detector, where photons that are "out-of-phase" might be observed to interfere due to the response characteristic of the detector or amplifier.

Starting with the first Rayleigh–Sommerfeld diffraction formula, the electromagnetic field amplitude at a screen or detector at X, Y, Z is $U(X, Y, Z)$, where the square of the amplitude is proportional to the energy flux or flux of photon particles. This formulation is reviewed in multiple texts on optical diffraction.[19,30,38] If this flux is normalized across the distribution, it can be used to provide probabilities for detection of photons. The first integral formula is

$$U(X, Y, Z) = \frac{1}{i\lambda} \int_{-\infty}^{\infty} \int_{-\infty}^{\infty} U(x, y, 0) \frac{Z}{r} \frac{\exp(ikr)}{r} dx\, dy, \quad (5)$$

where λ is the wavelength, k is the wavenumber, $k = 2\pi/\lambda$, and r is the vector length from the deflection point $(x, y, 0)$ in the aperture plane to the detection point at (X, Y, Z). $U(x, y, 0)$ is the field amplitude of the light crossing the area differential within the aperture at $(x, y, 0)$. This formalism assumes a dispersion of spherical waves, each of which emanates from the points $(x, y, 0)$, which are known as the Huygens wavelets. Fresnel introduced an additional obliquity factor to bias the propagation of these wavelets to the forward or z-direction. We note that optical theory assumes this dispersion but does not actually provide a basis for it. Thus, we need to establish a more physical foundation for our light scattering. Our effort is to look for an alternative, more-physical conceptualization that retains the demonstrated predictability of the Huygens–Fresnel principle.

The Kirchoff approximation to the integral integrates only over the area of the aperture. With the dispersion of light at $(x, y, 0)$, the propagation vector has a length

$$r = Z\left[1 + \frac{(X - x)^2 + (Y - y)^2}{Z^2}\right]^{1/2}. \quad (6)$$

We can use the binomial series expansion for r to obtain the Fresnel approximation applicable in the region, where Z is large relative to the wavelength and the x and y terms

$$r \cong Z + \frac{(X - x)^2 + (Y - y)^2}{2Z}. \quad (7)$$

This approximation thus assumes $Z \cong r$. Equation (5) becomes

$$U(X, Y, Z) = \frac{\exp ikZ}{i\lambda Z} \int_{-\infty}^{\infty} \int_{-\infty}^{\infty} U(x, y, 0) \exp\left[\frac{i\pi}{\lambda Z}(X - x)^2 \right.$$
$$\left. + \frac{i\pi}{\lambda Z}(Y - y)^2\right] dx\, dy. \quad (8)$$

This formalism adopts the Fresnel phase-shift of $-i = \exp{-i\pi/2}$ into the integral that is necessary for COW to align the theoretical predications with the experimental observations, though it also has an unclear physical basis.

As pointed out by many authors, the form of Eq. (8) provides a Fourier transformation of the field flux and is a two-dimensional convolution with respect to x and y. The exponentials correspond to the transfer function.[38–41] As the momentum of a photon can be expressed in terms of the wavenumber or wavelength, I will make this relation explicit in our analysis by the substitution, $p = h/\lambda$. I also note that the momentum deflections along the x and y axes can be represented by

$$\Delta p_x = p \sin \theta = p\frac{(X-x)}{r} \cong p\frac{(X-x)}{Z}, \qquad (9)$$

$$\Delta p_y = p \sin \phi = p\frac{(Y-y)}{r} \cong p\frac{(Y-y)}{Z}. \qquad (10)$$

These substitutions provide a momentum representation to our scattering equations (Huygen's wavelets) and are extremely useful to illustrate the connection between particle diffraction and momentum transfer. I have assumed the photon scattering to be elastic—the energy and wavelength of light is not changed. Making these substitutions and separating the exponentials

$$U = \frac{\exp iZ2\pi p/h}{i\lambda Z}\int_{-\infty}^{\infty}\int_{-\infty}^{\infty} U(x,y,0)\exp\left[i\pi\lambda Z\left(\frac{\Delta p_x}{h}\right)^2\right.$$
$$\left. + i\pi\lambda Z\left(\frac{\Delta p_y}{h}\right)^2\right]dx\,dy. \qquad (11)$$

Though we have not represented the polarization of our light in terms of electric and magnetic field vectors, the transverse electric field would lie in the x, y plane, thus our momentum exchange is allowed in this plane.

Assuming the illumination, $U(x, y, 0)$, is uniform over the aperture under consideration allows us to separate the integral

$$U(X,Y,Z) = U(0)\frac{\exp(iZ2\pi p/h)}{i}$$
$$\times \left[\frac{1}{\sqrt{\lambda Z}}\int_x \exp i\pi\lambda Z\left(\frac{\Delta p_x}{h}\right)^2 dx\right]$$
$$\times \left[\frac{1}{\sqrt{\lambda Z}}\int_y \exp i\pi\lambda Z\left(\frac{\Delta p_y}{h}\right)^2 dy\right]. \qquad (12)$$

We here see how the conversion to a momentum representation has demonstrated that the scattering integrals are dependent upon variables within the perpendicular x, y plane. We recognize that conservation of momentum along the z-axis should have some effect on the scattering probabilities, further confirming that Eq. (12) must be considered an approximation.

4 Single-Slit Diffraction

There are several aperture configurations for which solutions to the Rayleigh–Sommerfeld formula have been examined in detail. Analytical solutions to various aperture problems have been examined in detail by Steane and Rutt.[41] One familiar example is a long narrow slit, d wide, running along the y-axis, and centered at $x = 0$. The separate integrals of Eq. (12) are solvable in the traditional fashion using the Fresnel integrals,[42] integrating over x from $-d/2$ to $d/2$ and assuming the y integral from $-\infty$ to $+\infty$ gives a constant. (Note: this assumption that the y integral provides a constant, uniform dispersion is acceptable for uniform illumination but would not be accurate for a narrow laser beam; see Fig. 6.) Noting Eqs. (9) and (10), integration can be done with the substitution in the argument of $v = \sqrt{2Z/\lambda}\sin\theta$ and $v' = \sqrt{2Z/\lambda}\sin\phi$ and using the Cornu spiral, integral tables, or computer algorithms to generate numerical solutions.
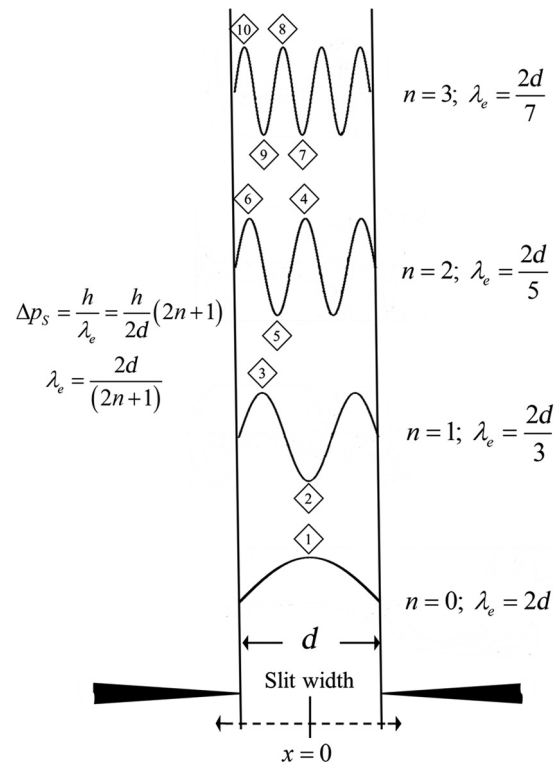
In the long distance, Fraunhofer limit for slit diffraction, the angular distribution for the intensity, I_X, exhibits the relation

$$I_X \propto \operatorname{sinc}^2[(d\pi p/h)\sin\sigma] \quad \text{where} \ \operatorname{sinc}\mu = \frac{\sin\mu}{\mu}, \ \operatorname{sinc}(0) = 1,$$
$$\qquad (13)$$

where σ is the angle of rotation of a ray from the origin of the aperture to $(X, 0, Z)$. This shows the primary dependence for this rotation on the width of the slit. This sinc function has extrema when the sine function has the value $\pi(n + 1/2)$ and is zero when the sine is $\pi(n + 1)$, where $n = 0, \pm 1, \pm 2, \pm 3, \ldots$. Substituting the momentum deflection, $\Delta p_x = p \sin \sigma$, maxima in the probability of the deflection of a photon occur whenever

$$\Delta p_x = p \sin \sigma = \Delta p_S = \frac{h}{2d}(2n+1) = \frac{h}{\lambda_e} = \hbar k_e, \qquad (14)$$

where λ_e is an "effective wavelength" and k_e is an "effective wavenumber," useful geometric parameters that we can associate with a momentum transfer to the photon at the aperture. There are higher probability values for this effective wavelength when it is an odd fraction of $2d$. We recognize these momentum transfers parallel the momentum eigenvalues from the analysis of a one-dimensional square well (particle-in-a-box) using Schrödinger's wave equation.[8–10] This connection is visualized in Fig. 2, where the wave-like solutions

$$\Delta p_S = \frac{h}{\lambda_e} = \frac{h}{2d}(2n+1)$$

$$\lambda_e = \frac{2d}{(2n+1)}$$

$n = 3; \ \lambda_e = \dfrac{2d}{7}$

$n = 2; \ \lambda_e = \dfrac{2d}{5}$

$n = 1; \ \lambda_e = \dfrac{2d}{3}$

$n = 0; \ \lambda_e = 2d$

d

Slit width

$x = 0$

Fig. 2 Single-slit diffraction in the Fraunhofer limit. The effective wavelength for momentum transfer, λ_e, is shown for four different values of n corresponding to maxima in the diffraction pattern. These are related to geometrically harmonic solutions to Schrödinger's wave equation for a one-dimensional square well. The significance of the numbered inflection points is described later in Table 2.
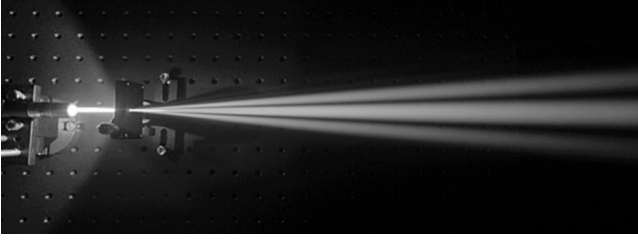
Fig. 3 Green (520 nm) laser pointer diffracted by a narrow slit with beam illuminated by a fog generator. Picture illustrates the probabilities of the paths for scattered photons. (Credit: Quantum Optics Lab Olomouc 2012.)

for a square well of width, d, ($\psi_S = A \cos 2\pi x/\lambda_e$) are shown with the corresponding values of λ_e for the first four values of n.

Figure 3 is a picture of a green laser pointer diffracted by a single, narrow slit, where the paths for the scattered photons are illuminated by a water vapor fog. This type of experimental set up helps to illustrate how the photon paths are determined at the slit aperture, though the scattering pattern can be predicted by the formalism of a wave.

In single-slit experiments examining the near-field, there appears a minima in the center of the diffraction pattern (see Harris et al.[26]). Fresnel's criteria for such minima assume that the integration is over four Fresnel zones. I have pointed out previously that to obtain such a pattern, the magnitude of momentum transfer must be dependent on the position within the slit as well as specific momentum eigenvalues of the slit.[6] This relation will be clarified through our examination of straight-edge diffraction.

5 Straight-Edge Diffraction

The classical derivation of the scattering intensity at a distant screen for edge diffraction of monochromatic light can be found in most optics textbooks.[19,42] The derivation usually employs the Rayleigh–Sommerfeld and Fresnel–Kirchoff theories of diffraction. The experimental setup is illustrated in Fig. 4, with a long, straight edge located at $x = 0$.

(a)

(b)
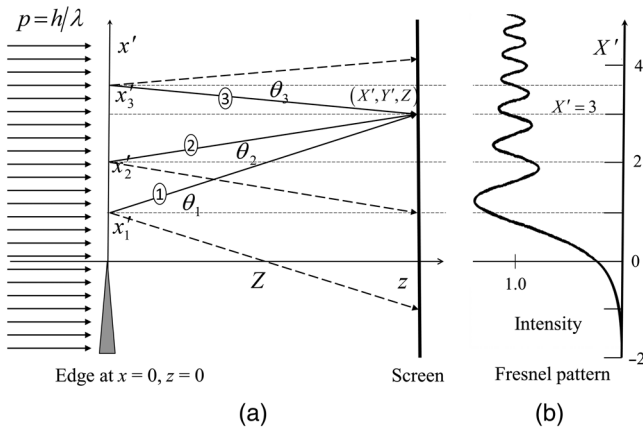
Fig. 4 (a) Diagram of Fresnel diffraction of monochromatic light by a long, straight edge at $x = 0$, $z = 0$, and distant detector screen at $z = Z$. The six different photon scattering trajectories are shown, where $\Delta p_x = \mathbf{g}h/x$, $\mathbf{g} = 1$ from Eq. (27), three converging at the detection point, X, Y, Z. (b) Typical Fresnel intensity pattern produced by edge on distant screen.

From the first Rayleigh–Sommerfeld diffraction formula, Eq. (5), we have derived the illumination field, $U(x, y, 0)$, in Eq. (12). For edge diffraction, integration over the y-dimension will generate a constant that can be combined in the coefficient, thus, we can focus on the x dependence. Using a familiar substitution, we obtain as follows

$$
\nu = -\sqrt{2\lambda Z}\frac{\Delta p_x}{h} = -\sqrt{\frac{2Z}{\lambda}}\sin\theta \cong -\sqrt{\frac{2}{\lambda Z}}(X - x)
$$
$$
= -(X' - x'), \tag{15}
$$

and also use the simplification

$$
X = X'u; \quad x = x'u, \quad \text{and} \quad u = \sqrt{\lambda Z/2}, \tag{16}
$$

where u is the Fresnel scaling factor or coefficient that will define our dimensional units. The field amplitude is proportional to our revised integral

$$
U(X', Y', Z') = -iW(0) \int_\nu \exp\left(\frac{i\pi\nu^2}{2}\right) d\nu, \tag{17}
$$

where the integration is from $x' = 0 \to \infty$; thus, $\nu = -X' \to \infty$. As demonstrated in standard texts,[37,42] the exponential can be separated into a cosine and sine function and solved using the familiar Fresnel integrals, where

$$
C(\nu) \equiv \int_0^\nu \cos\left(\frac{\pi\nu^2}{2}\right) d\nu \quad \text{and} \quad S(\nu) \equiv \int_0^\nu \sin\left(\frac{\pi\nu^2}{2}\right) d\nu. \tag{18}
$$

Thus,

$$
U(X', Y', Z') = -iW(0)\{C(\infty) - C(-X')
$$
$$
+ i[S(\infty) - S(-X')]\}, \tag{19}
$$

and the irradiance (intensity) is proportional to the complex square

$$
I_{X'} \approx U^2(X', Y', Z')
$$
$$
= W^2(0)\{[C(\infty) - C(-X')]^2 + [S(\infty) - S(-X')]^2\}, \tag{20}
$$

or using the uniform unobstructed irradiance, $\Phi(x_0')$, as our proportionality constant

$$
I_{X'} = \frac{\Phi(x_0')}{2}\left[\begin{array}{c} C^2(\infty) - 2C(-X')C(\infty) + C^2(-X') \\ +S^2(\infty) - 2S(-X')S(\infty) + S^2(-X') \end{array}\right]
$$
$$
= \Phi(x_0')A_{X'}. \tag{21}
$$

Having used a standard derivation from COW, we can further deconstruct the components to these equations. In the illuminated region, where X' is positive, we can separate this irradiance approximation into the sum of two functions representing attractive and repulsive deflections. These component functions are plotted in Fig. 5

$$
\frac{I_{X'}}{\Phi(x_0')} = A_{X'} = B_{X'} + \Gamma_{X'}, \tag{22}
$$
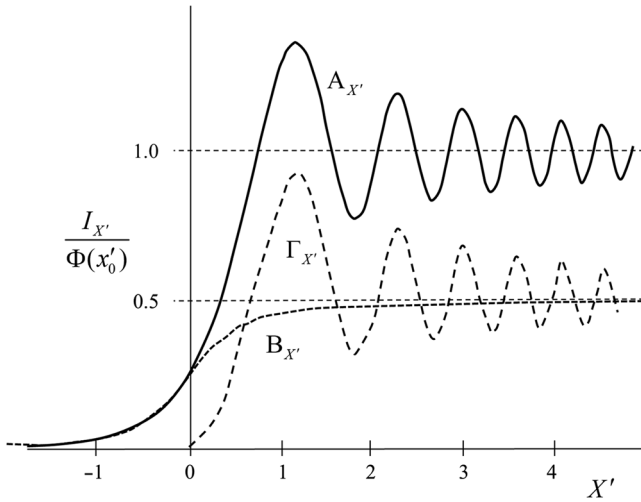
Fig. 5 Contributions to the observed diffraction pattern from a straight edge, $A_{X'}$. $\Gamma_{X'}$ is the relative contribution from repulsive, positive deflections, Eq. (24), and $B_{X'}$ is the relative contribution from attractive, negative deflections, Eq. (26). $\Omega_{X'}$ is a derived component of $\Gamma_{X'}$ defined in Eq. (35).

where the sum of the repulsive, positive deflections is estimated by

$$\Gamma_{X'} = \frac{1}{2}[2C^2(-X') + 2S^2(-X')] = [C(-X') + iS(-X')]^2, \tag{23}$$

$$\Gamma_{X'} = \left[\int_{\nu=0}^{X'} \exp\left(\frac{i\pi\nu^2}{2}\right)d\nu\right]^2. \tag{24}$$

The approximate sum of the attractive, negative deflections is calculated as the difference as follows

$$B_{X'} = A_{X'} - \Gamma_{X'} = \frac{1}{2}\left[\begin{array}{c}2C^2(\infty) + 2S^2(\infty) - [C(\infty) \\ + C(-X')]^2 - [S(\infty) + S(-X')]^2\end{array}\right], \tag{25}$$

$$B_{X'} = \left[\int_0^\infty \exp\left(\frac{i\pi\nu^2}{2}\right)d\nu\right]^2 - \frac{1}{2}\left[\int_{X'}^\infty \exp\left(\frac{i\pi\nu^2}{2}\right)d\nu\right]^2$$
$$= \frac{1}{2} - \frac{1}{2}\left[\int_{X'}^\infty \exp\left(\frac{i\pi\nu^2}{2}\right)d\nu\right]^2, \tag{26}$$

when $X' \geq 0$. Thus, we can construct the irradiance in terms of the sum of two integral functions; one determined from zero to X' and the other from X' to ∞. This again displaces the idea that the irradiance is a result of interference at a detection point by demonstrating that it can be the sum of multiple dispersion terms defined at a scattering lattice.

Fresnel provided us with two useful conceptual tools to describe the summation and interference of Huygens wavelets. One is the Fresnel number associated with the scattering to X, Z, where $N_F = X^2/\lambda r \cong X'^2/2$. We note the integral, $\Gamma_{X'}$, spans the phase interval, N_F. A second, related tool is the Fresnel half-period zones analysis. The half period zones define the dimensional spacing at the scattering object or aperture that correspond to half-period phase differences in dispersed wavelets reaching a specific detection point. Insight to our edge diffraction is gained referencing these tools. MET relates these to momentum exchange criteria.

Table 1 provides the relevant dimensions for a Fresnel zones analysis of our edge diffraction experiment. The dimension from $x = 0$ to the edge of each Fresnel half-period zone is calculated such that there is a half-period difference at Z, column B. We note that these zone edges approximate the X' inflection points in our analysis of the diffraction pattern of Fig. 5, column E. Also calculated, related to Eq. (4), is the effective wavelength that would be associated with a momentum exchange at the aperture that leads to a photon deflection equal to the length to the zone edge, column C. Our definition of the momentum exchange coefficient that can be related to the Fresnel number, column D, will be developed in the next section that clarifies how these are connected to the calculated coefficient at the profile inflection points, column F.

Table 1 Parameters associated with a Fresnel analysis of edge diffraction in Fresnel units. Description of each column is provided in the text.

	Fresnel zones analysis			Fresnel integrals analysis	
A	B	C	D	E	F
Fresnel zone # m	Zone edge $x'_m = \sqrt{2m}$	Zone edge momentum exchange $\lambda'_e = \sqrt{2/x'_m}$	Exchange coefficient $g_m = X'^2_m/8 = m/4$	Calculated inflection points X'	Coefficient at inflection point $g = X'^2/8$
1	$\sqrt{2}$	$\sqrt{2}$	1/4	1.2	0.18
2	$\sqrt{4}$	$\sqrt{4}/2$	1/2	1.9	0.43
3	$\sqrt{6}$	$\sqrt{6}/3$	3/4	2.3	0.69
4	$\sqrt{8}$	$\sqrt{8}/4$	1	2.7	0.94
5	$\sqrt{10}$	$\sqrt{10}/5$	5/4	3.1	1.20
6	$\sqrt{12}$	$\sqrt{12}/6$	6/4	3.4	1.45

6 Phenomenological Description and Experimental Curve Fitting

Converting to a momentum representation gives us an alternative interpretation for optical diffraction formulas in terms of momentum exchange corresponding to microwave energies. We demonstrated the irradiance predications of COW can be constructed as the sum of attractive and repulsive momentum exchange terms. In this next section, we will "reverse engineer" these terms, assuming that they represent the experimentally observed diffraction patterns and develop the momentum exchange descriptions that will generate these patterns. This analysis makes a few simple assumptions: (a) photons behave as particles with specific paths and quantized momentum; (b) photons are scattered in the vicinity of an aperture or lattice by momentum transfer with that lattice; (c) the momentum transfer probabilities are defined by two factors: (1) the momentum exchange states associated with the lattice and (2) the distance over which momentum is transferred.

The probability for scattering in MET must result from a distinct ensemble of exchange potential functions within the aperture and their cross-section at the path point of photon scattering. Such an assumption is necessary to generate the sharp definition of optical diffraction patterns. We note that BDW theory draws upon the geometry and symmetry of the scattering boundary or aperture to define the interference with the incident wave.[33] For example, Schwinger et al.[43] use the "more physical" approach of BDW and describe the scattered wave by a long, straight edge as a cylindrical field, concentric to the edge. We make the distinction between MET and BDW in that the field in the proximity of the edge or aperture determines the scattering and not interference at the point of detection as in BDW.

The similar symmetry requirements may be clarified by our observation of the scattering of a laser beam by a long, narrow slit. Note, in Fig. 6, the laser light is scattered perpendicular to the length of the slit. The scattering field contributions parallel to the edge must cancel or not contributed—the parallel scattering is no wider than the original beam.

In determining how these fields/potentials interact, we will make an analogy to Thomson scattering by an electromagnetic field in x-ray crystallography, where the structure factor for a crystal's geometry is expressed in a reciprocal phase space that defines x-ray reflections.[44] This reciprocal space representation can be correlated to momentum eigenfunctions of the crystal lattice that determine the scattering profile. We should be able to define optical scattering from an aperture in terms of a reciprocal geometry that is correlated with momentum transfer states. A difference from crystallography is that we do not immediately recognize

Fig. 6 Photo of observed diffraction pattern for a He–Ne laser through a 0.1-mm vertical slit. Photon scattering is perpendicular to the slit. (Credit: Jordgette 2010.)

a periodic pattern of the scattering electromagnetic field in reciprocal space. Our analysis will help us converge on the scattering probabilities for this momentum transfer in the plane of an aperture.

Our analysis of edge diffraction will assume that the momentum transfer is a reciprocal function of the distance, x, between the photon path and edge of the aperture. As with our analysis for Eq. (21), we assume a summation of deflected photon paths that converge upon the screen point $(X, 0, Z)$ scattered from points in the plane of the aperture, $(x, 0, 0)$ and thus, $\Delta x = (X - x)$. As with BDW analysis and experimental observations, we assume the y-contributions to deflections will cancel. Making the substitution, $\Delta p_x = gh/x$, into Eq. (9), the net potential momentum transfer with an exchange coefficient, g, is expressed by

$$\Delta p_x = p \sin\theta = \hbar k_e = \frac{h}{\lambda_e} = \frac{gh}{x} = \frac{h(X-x)}{\lambda r} \cong \frac{h(X-x)}{\lambda Z};$$
$$g \cong \frac{(X'-x')x'}{2}. \tag{27}$$

The diffraction pattern will be determined by the probabilities for the different positive and negative values of g. Expressing distances in terms of the Fresnel coefficient, u, we solve Eq. (27)

$$x' \cong \frac{X'}{2} \pm \frac{\sqrt{X'^2 - 8g}}{2}, \tag{28}$$

providing the multiple values to x' that would deflect to X' for a particular coefficient, g. When g is positive, there are two real solutions for x' when $X'^2 > 8g$, and only one real solution when g is negative. I have depicted the three different solutions for x' that will deflect to $X' = 3$ in Fig. 4, when $g = \pm 1$. The intensity or photon flux at each value of X' is generated using the differentials, Eq. (29), and knowing the flux at each value of x'. We will assume the intensity at x', $I = \Phi(x')dx'$, where $\Phi(x')$ is the flux for unit length, Δy, at x' from the edge. The differential is used to relate the cross-section and flux at x' to the intensity at X'

$$\frac{dx'}{dX'} \cong \left(\frac{1}{2} \pm \frac{X'}{2\sqrt{X'^2 - 8g}}\right). \tag{29}$$

For each absolute value of g, there can be up to three different values of x' that deflect to each value of X'. We can determine the contribution to the intensity from each deflection cross-section. For g positive, a positive deflection (repulsion) from the edge, we obtain

$$x_1' \cong \frac{X'}{2} - \frac{\sqrt{X'^2 - 8g}}{2}; \qquad x_2' \cong \frac{X'}{2} + \frac{\sqrt{X'^2 - 8g}}{2}, \tag{30}$$

where $X'^2 > 8g$. The intensity contribution at X', $I(+g)$, from these deflections will be a function of the probability for a particular value of g, $\Pr(+g)$

$$I(X', +g) = \Phi(x_1') \Pr(+g) dx_1'/dX' + \Phi(x_2') \Pr(+g) dx_2'/dX'$$
$$= \Phi(x_1') \Pr(+g) \left| \left(\frac{1}{2} - \frac{X'}{2\sqrt{X'^2 - 8g}} \right) \right|$$
$$+ \Phi(x_2') \Pr(+g) \left| \left(\frac{1}{2} + \frac{X'}{2\sqrt{X'^2 - 8g}} \right) \right|. \quad (31)$$

Here, I have used the convention in physics to take the absolute value of the differential cross-section, so that the flux contributions will sum positively. This provides a generic equation allowing us to calculate the intensities when the illumination is not uniform. The intensity contribution at X' from positive deflections will be the sum (integral) of the contributions from the different values of x' from 0 to X'

$$I(X') = \int_{x'=0}^{X'/2} \Phi(x_1') \Pr(+g) \left| \left(\frac{1}{2} - \frac{X'}{2\sqrt{X'^2 - 8g}} \right) \right| dx'$$
$$+ \int_{x'=X'/2}^{X'} \Phi(x_2') \Pr(+g) \left| \left(\frac{1}{2} + \frac{X'}{2\sqrt{X'^2 - 8g}} \right) \right| dx',$$
$$I(X') = \int_{g=0}^{g=X'^2/8} \Phi(x_1') \Pr(+g) \left| \left(\frac{1}{2} - \frac{X'}{2\sqrt{X'^2 - 8g}} \right) \right| dg$$
$$+ \int_{g=X'^2/8}^{g=0} \Phi(x_2') \Pr(+g) \left| \left(\frac{1}{2} + \frac{X'}{2\sqrt{X'^2 - 8g}} \right) \right| dg. \quad (32)$$

If we assume the illumination beyond the edge is uniform, expressed by the unobstructed intensity, $\Phi(x_0')$, Eq. (32) reduces to

$$I(X', +g) = \Phi(x_0') \Pr(+g) \left[\frac{X'}{\sqrt{X'^2 - 8g}} \right]. \quad (33)$$

This provides our basis to calculate $\Pr(+g)$ by fitting to our experimental observations. Equation (33) correlates with Eq. (24) that relates to our positive deflections. Assuming Eq. (24) reflects an observed experimental profile, we connect these relations

$$\Gamma_{X'} = \frac{I_{X'}(+g)}{\Phi(x_0')} = \int_{+g} \Pr(+g) \left[\frac{X'}{\sqrt{X'^2 - 8g}} \right] dg$$
$$= \int_{+g} \Pr(+g) \left(1 - \frac{8g}{X'^2} \right)^{-1/2} dg. \quad (34)$$

We note the integral will only be real for $g \leq X'^2/8$, so our integration is limited to $g = 0 \rightarrow X'^2/8$. As g approaches $X'^2/8$, our denominator approaches infinity. We can approximate the square root term by a series expansion and adding a delta function, Δ, as g approaches $X'^2/8$

$$\Gamma_{X'} = \int_{g=0}^{X'^2/8} \Pr(+g) \left[1 + \Delta \left(\frac{X'^2}{8} - g \right) \right] dg$$
$$= \int_{g=0}^{X'^2/8} \Pr(+g) dg + \beta \Pr \left(g = \frac{X'^2}{8} \right)$$
$$= \Omega_{X'} + \beta \Pr \left(g = \frac{X'^2}{8} \right), \quad (35)$$

where β is a constant from the integration of the delta function. We can use Eq. (35) to generate $\Pr(+g)$ by mathematical iteration and curve fitting techniques. We can make a first-order approximation for $\Pr(+g)$ assuming a near fall-off from $g = 0$, thus the first term of Eq. (35) will generate a smooth curve going from 0 to ½ as $X'^2/8$ increases. Such an approximate curve is shown as $\Omega_{X'}$ in Fig. 5. Subtracting Ω from Γ gives us, $\beta \Pr(X'^2/8)$, our relative probability. Using $g = X'^2/8$ gives the relative probability distribution for positive g that is plotted in Fig. 7.

Though this curve in Fig. 7 can be derived from experimental observations, we have correlated it to calculated Fresnel pattern of Fig. 4 and the resulting inflection points are tabulated in Table 1. By connecting these relations, we observe the harmonic probability profile in Fig. 7(a) can be modeled by a diminishing function with a frequency approximated by the form
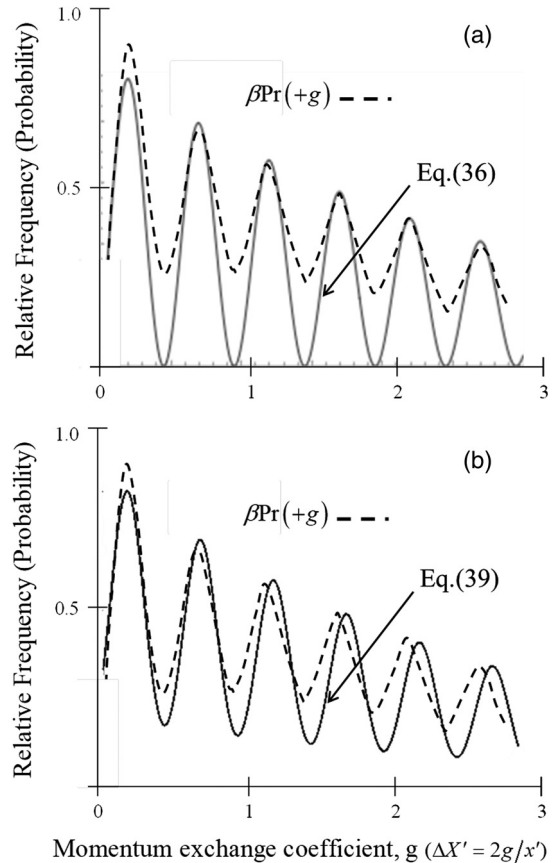
Fig. 7 Relative probability distribution for the different values of g (dashed). The distribution for positive g is obtained by fitting the momentum exchanges of Eqs. (33) and (35) to the curve, $\Gamma_{X'}$, of Fig. 5. The shape of this profile can be confirmed experimentally. (a) Solid curve is the harmonic function in Eq. (36). (b) Solid curve is the sum of Gaussian distributions at $+g$ maxima in Eq. (39).

$$\Pr(+\mathrm{g}) \propto \cos^2 \pi\left(\frac{X'^2}{4} - \frac{b}{2}\right) \times \exp\left(\frac{-X'^2}{8a}\right)$$

$$= \cos^2 \pi\left(2g - \frac{b}{2}\right) \times \exp\left(\frac{-|g|}{a}\right), \qquad (36)$$

with a and b used to fit to the curve. Local minima and maxima are as follows

$$4g - b \cong m - 1, \qquad g \cong \frac{(m-1)}{4} + \frac{b}{4}, \qquad (37)$$

where $m = $ Fresnel zone number, 1,2,3,... From experimental curve fitting of Eq. (36), $b \cong 0.8$ and $a \cong 3$. The higher probability points (maxima) shown in Table 1 are when the Fresnel zone numbers are odd, or alternatively when

$$g \cong \frac{j}{2} + 0.2, \quad \text{where} \quad m = 2j + 1, \quad j = 0,1,2,3,\ldots. \qquad (38)$$

The local maxima are at increments of $\Delta p = h/2x$. Alternatively, these probability maxima for g might be associated with momentum transition states for the aperture with behavior resembling spectral lines with broadening defined by Gaussian or Lorentzian statistical distributions. In this case, we might model the probability of $+g$ by a summation resembling

$$\Pr(+\mathrm{g}) \propto \sum_j c_j \exp\frac{-[g - (2j + b)/4)]^2}{w^2}, \qquad (39)$$

where the coefficients, c_j, may correspond to the density of accessible states. This is plotted in Fig. 7(b) with the curve fitting of $c_j = \exp{-[(1/a)(2j + b)/4]}$, $b \cong 0.8$, and $w = 0.17$.

Though our curve fitting set $b \cong 0.8$, for insight to the geometric selection rules for momentum exchange and the Fresnel zone analysis of optical theory, we will examine setting $b = 1$, such that the inflection points for g correspond to $g = m/4$. These track the values for g_m in Table 1, column D. The probability of Eq. (36) then relates to the sine function

$$\Pr(+\mathrm{g}) \propto (\sin^2 2\pi g) \exp\left(\frac{-|g|}{a}\right)$$

$$= (\sin^2 \mathrm{k}_e \cdot x) \exp\left(\frac{-|\mathrm{k}_e \cdot x|}{2\pi a}\right). \qquad (40)$$

Local maxima in momentum exchange from Eq. (27) are thus approximated where

$$\Delta p_x = \hbar \mathrm{k}_e = \frac{h}{\lambda_e} = g\frac{h}{x} \cong \frac{(2j + 1)h}{4x},$$

and thus $x \cong \frac{2j + 1}{4}\lambda_e$. $\qquad (41)$

From Eq. (41), the higher probabilities for momentum exchange are found when the effective wavelength is an odd fraction of $4x$. This relation illuminates the connection between the momentum exchange selection rules and the
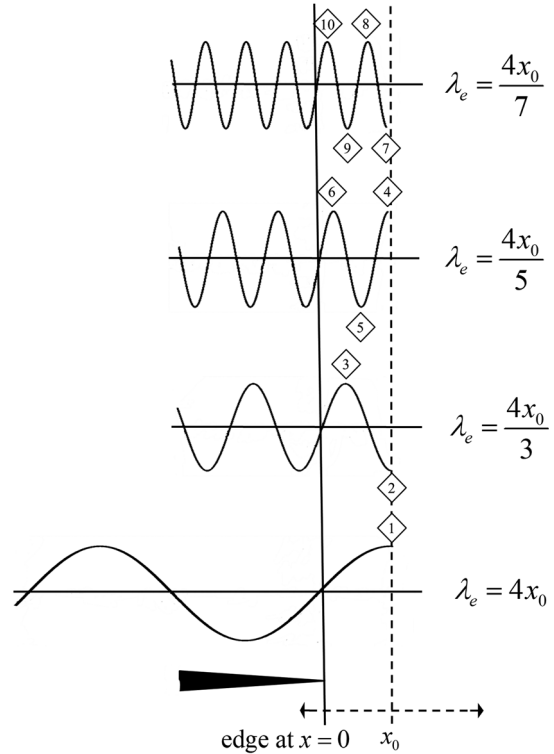
Fig. 8 Straight-edge diffraction. Graphical representation of four solutions to Eq. (41), where momenta exchange are maxima. Superimposed on the x-axis is $\sin 2\pi x/\lambda_e$ for the different values of the effective wavelength for momentum exchange, λ_e. The photon path is at x_0 from the edge.

Fresnel phase-shift of $-\pi/2$ adopted in Eq. (5). With Eq. (40), we come full-circle on our predictions of Sec. 2.4, demonstrating diffraction as a harmonic function of momentum transfer in the plane of the aperture.

The relationship between the effective wavelength for momentum exchange and the distance to the edge is graphically illustrated in Fig. 8, where a sine function for different solutions for λ_e in Eq. (41) is superimposed on the x-axis of our edge experiment with the value set to 0 at $x = 0$. We note in Fig. 8 how the selection rules for momentum exchange identify an effective wavelength (momentum) that relates to the exchange distance to the photon path. This suggests a geometric relationship between the properties of the momentum exchange particles or electromagnetic potential near the aperture and the path of the scattered photons.

When we bring two long, straight edges toward each other, we create a single-slit diffraction configuration. We can directly relate the predicted exchange maxima from Fig. 8 with the single-slit scattering predictions shown in Fig. 2. We assume a slit separation, d. We can equate the relations for the maxima in the effective wavelength probabilities for both experimental configurations

$$\lambda_e = \frac{2d}{(2n + 1)} = \frac{4x}{(2j + 1)}; \qquad |j| \le |n|. \qquad (42)$$

Thus, the maxima in the probability for exchange are observed when the values for x, the distance from the photon path to the edge, are given by

Table 2 Equating the maxima in the probabilities for the effective wavelengths for single-slit and straight-edge diffraction allows us to calculate the distance of the photon path from the edge for these momentum transfers. Position numbers correspond to the location of the inflections at these values of x in Figs. 2 and 8.

λ_e	n	j	x from edge	Figs. 1 and 7 position #
$2d$	0	0	$d/2$	1
$2d/3$	1	1	$d/2$	2
$2d/3$	1	0	$d/6$	3
$2d/5$	2	2	$d/2$	4
$2d/5$	2	1	$3d/10$	5
$2d/5$	2	0	$d/10$	6
$2d/7$	3	3	$d/2$	7
$2d/7$	3	2	$5d/14$	8
$2d/7$	3	1	$3d/14$	9
$2d/7$	3	0	$d/14$	10

$$x = \frac{d(2j+1)}{2(2n+1)}. \tag{43}$$

These positions correspond to the inflection points for the sinusoidal functions plotted in Figs. 2 and 8. The calculations for the different values for n and j are shown in Table 2. This table shows the values for x associated with these maxima and provides a number label for these inflection points in the figures. The values for n define the momentum eigenvalues for the maxima in exchange and the values for j define the distance of the photon paths from the edge that will

exchange momentum with these values. The square of the harmonic functions plotted in Figs. 2 and 8 is related to the probability of momentum exchange at each point. We note the amplification of specific values of λ_e from multiple paths. Scattering solutions are shown for half of the single slit as each half is symmetric. The total dispersion (diffraction pattern) would be the sum across all points in the slit.

This diffraction by a narrow slit is sketched in Fig. 9 for a configuration in the near-field, where the half width of the slit, $d/2$, is equal to two Fresnel zones (total of four over slit), $Z \cong d^2/8\lambda$. The figure depicts the higher probability scattering trajectories only from positions 1 through 6 labeled in Fig. 2 and Table 2. The magnitudes of the deflections are defined by the effective wavelengths for momentum exchange, column one of Table 2. Figure 9 helps us visualize how this momentum exchange scattering can replace the concept of Huygens wavelets produced at the aperture. At $d/2$, there is the highest probability for scattering and the most probable six deflections are shown. Figure 9 illustrates how we would see an intensity minima at the center of the profile for this screen distance, as predicted by Fresnel and experimentally documented (see Harris et al.[26]). In the far-field, Fraunhofer limit where the intensity profile can be described by Eq. (13), the peak in the center of the profile corresponds to $n = 0$, $j = 0$, and $g = 1/4$. In this case, the momentum exchange determining this center is $\Delta p_S = \pm h/4x$, for each half-slit width from $x = 0$ to $d/2$.

7 Multiple Slits and Talbot Effect

We may examine the COW treatment of multiple-slit diffraction provided by Born and Wolf[1] that merges the intensity profile for a single-slit with that for multiple slits [see Eqs. (13) and (14)]

$$I_X \propto \left[\frac{\sin N(L\pi p/h) \sin \sigma}{\sin(L\pi p/h) \sin \sigma} \right]^2 \mathrm{sinc}^2[(d\pi p/h) \sin \sigma], \tag{44}$$
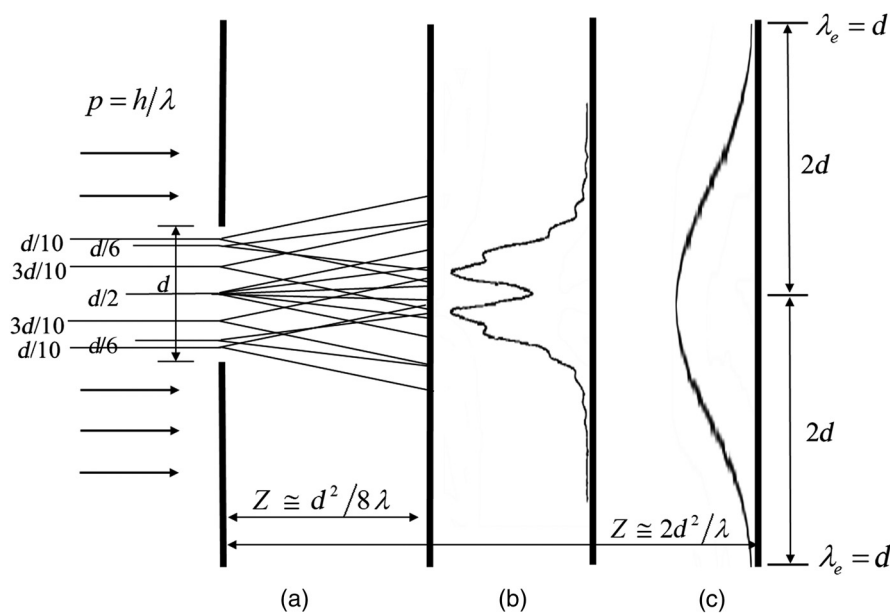
Fig. 9 (a) Deflection of parallel light paths from different positions within a single slit of width d. Higher probability deflections correspond to positions 1 through 6 in Fig. 2 and Table 2. (b) Fresnel intensity pattern at a distance $Z \cong d^2/8\lambda$ from the aperture corresponding to $\sim$4 Fresnel zones. (c) Intensity pattern at $Z \cong 2d^2/\lambda$, one Fresnel zone, first minima at $2d$ from center where $\lambda_e = d$ (see intensities in Harris et al.[26]).
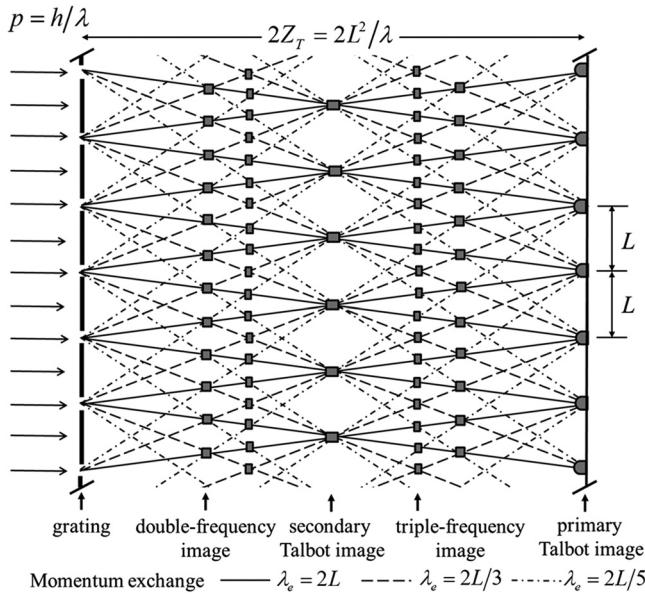
Fig. 10 The optical Talbot effect. Diagram of the dispersion of monochromatic light through an extended grating on left with narrow, parallel slits at increments of L. The six most probable momentum exchanges at each slit are shown as rays connecting to the primary Talbot image on the right. This illustrates the "Talbot carpet" with double-frequency and triple-frequency images.

where N is the number of equally spaced parallel slits. (The point for the zero angle of deflection is taken perpendicular to each slit.) The intensity has maxima when the denominator in the first term is zero; when the argument of the sine is zero or an integral multiple of π, whenever

$$\Delta p_x = p \sin \sigma = \Delta p_M = \frac{jh}{L}, \tag{45}$$

where j is an integer. Using an operator formalism more familiar to quantum mechanics, Van Vliet[20] recently updated the description of multiple-slit diffraction in terms of quantized momentum transfer in increments related to the slits' separation, L: $\Delta p = jh/L$, in alignment with classical optics.

Harris et al.[26] provide useful experimental results for double-slit optical diffraction in the far-field, where the slit separation (12.68 mm) is large compared to the slits' width (0.65 mm). The experimental intensity pattern is consistent with the theoretical predictions with deflection increments at $\Delta p = jh/L$. The pattern also exhibited the contribution of each of the narrow slits to the dispersion. We have seen from our analysis [Fig. 9(c)] that in the far-field, the most probable contribution to the scattering from a single slit corresponds to $\Delta p_S = \pm h/2d$, with these two dispersion profiles summing to a single peak distribution at the distant screen and additional peaks at $\Delta p_S = (2n + 1)h/2d$. With the existence of a second or multiple slits in the experiment, the dispersion with momentum exchange increments, $\Delta p = jh/L$, can be added to the single-slit profiles if an additional functional dependence is imposed as with Eq. (44). Equation (44) was suitable for the Fraunhofer region, but we would like to consider deflections in the nearer field, Fresnel region by integrating the phase shift of $\pi/2$ into our analysis. In this case, the most probable momentum deflections for the double slit would correspond to a form

$$\Delta p = \frac{(2n + 1)h}{2d} \pm \frac{(2j + 1)h}{2L}. \tag{46}$$

Similar to our analysis of a single slit in Fig. 2, we note that the most probable values for momentum exchange due to the slit separations also resemble the solutions to a one-dimensional square well, where the width of the well is $2L$ and the origin for the x dimension is centered at one slit

$$\psi_M = A \cos \frac{2\pi x}{\lambda_e} = A \cos \frac{2\pi x(2j + 1)}{2L}. \tag{47}$$

If, as with our single-slit analysis, the probability for momentum exchange at x is proportional to the square of this function, there is highest probability for momentum exchange with photons at each slit.

7.1 Talbot Effect

A comprehensive review of the Talbot effect and its many applications in modern optics has been presented by Wen et al.[45] The Talbot effect is associated with Fresnel diffraction of coherent, monochromatic light by an extended, multiple-slit grating, periodic in the transverse direction. The effect is observed in the formation of a perfect image of the grating (Talbot image or Fourier image) at a distance, $2Z_T = 2L^2/\lambda$ and a contrast reversed image (also a Talbot image) at $Z_T = L^2/\lambda$, where Z_T is referred to as the Talbot distance. These Talbot images have also been termed "Fresnel images" or "self images."

An optical experiment to observe the Talbot effect is sketched in Fig. 10. We may use the Fresnel–Kirchoff diffraction formula, Eq. (8), to derive a solution

$$U(X) \propto \int_{-\infty}^{\infty} U(x) \exp\left[\frac{i\pi}{\lambda Z}(X - x)^2\right] dx$$
$$= \int_{-\infty}^{\infty} U(x) \exp\left[i\pi\lambda Z\left(\frac{\Delta p_x}{h}\right)^2\right] dx. \tag{48}$$

Following Goodman's Fourier analysis,[19] the grating, with slits perpendicular to x, can be modeled as a transmitting structure with amplitude transmittance

$$U(x) = \frac{1}{2}\left[1 + q \cos\left(\frac{2\pi x}{L}\right)\right]. \tag{49}$$

I would note that if q is 1 [Eq. (49)], this transmission function has the same form as the square of our momentum eigenfunctions in Eq. (47)—these are Fourier frequency components of our grating geometry. This points to the clear connection between MET and the Fourier analysis to describe multiple-slit diffraction. Using a transfer function approach to develop a solution, the intensity distribution was found to be as follows

$$I(X) \propto 1 + 2q \cos\left(\frac{\pi\lambda Z}{L^2}\right)\cos\left(\frac{2\pi x}{L}\right) + q^2 \cos^2\left(\frac{2\pi x}{L}\right). \tag{50}$$

We observe when

$$\frac{\pi\lambda Z}{L^2} = 2\pi n \quad \text{or} \quad Z = \frac{2nL^2}{\lambda} = 2nZ_T, \tag{51}$$
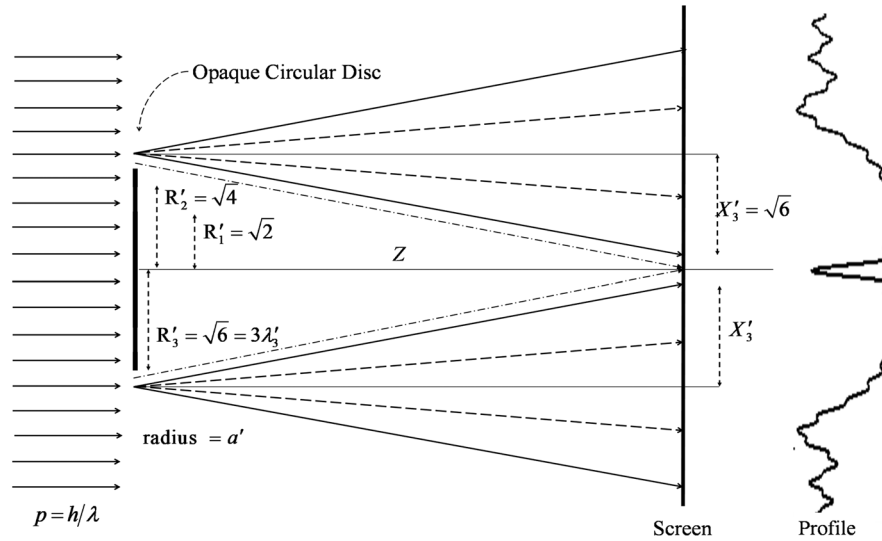
Fig. 11 Diffraction by an opaque circular disc with similar experimental conditions to Fig. 4. Different deflected photon paths are shown. Poisson's spot or spot of Arago is observed at the center of the shadow. Depicted is an experimental configuration, where the opaque disc has a radius of three Fresnel half zones (shown). Dimensions shown are in Fresnel units.

there is a perfect image of the grating reformed at the screen (see Fig. 10). At odd multiples Z_T, we see a contrast reversal with an intense spot whenever $x = (2j+1)L/2$. This is the secondary Talbot image. In Fig. 10, light rays representing the six most probable dispersions from each slit are drawn from each grating slit to these spots at Z_T. Dispersions between these rays must have low probability to retain the dark areas between these spots. We can calculate the higher probability momentum exchanges associated with the deflections of these rays. The effective wavelength, λ_e, for these transfers is

$$\lambda_e \cong \frac{\lambda Z}{\Delta x} = \frac{2\lambda Z_T}{(2j+1)L} = \frac{2L}{(2j+1)},$$

$$\Delta p_M = \frac{h}{\lambda_e} \cong \frac{(2j+1)h}{2L},$$

(52)

consistent with Eq. (46) and confirming the Talbot effect is due to quantized momentum exchange at the grating.

8 Diffraction by an Opaque Circular Disc: Poisson's Spot

We can learn more about the probabilities for momentum exchange by examining a very similar experiment, the diffraction by an opaque circular disc, which can give our experimental predictions for negative g. A typical experiment can be configured as our Fig. 4, replacing our long straight edge with a circular disc. This configuration is assumed in Fig. 11. This experiment has an interesting history. In 1818, Poisson used Fresnel's wave theory to predict a spot in the middle of a circular shadow, thereby suggesting that Fresnel's theory was absurd. This spot was later observed by Arago giving strong endorsement to Fresnel's wave theory of light in preference over Newton's corpuscular theory.[46] This observation has subsequently been referred to as Poisson's spot or the spot of Arago. It is useful to demonstrate that this spot can be explained in terms of photon dispersion through momentum exchange.

Lucke[47] has noted the problems of accurately predicting the intensity profile within the shadow of an opaque disc using the familiar wave theory diffraction integrals. He has demonstrated that the Rayleigh–Sommerfeld formulas can lead to accurate descriptions near the central axis, though the approximations become less accurate toward the edge. Lucke has also shown that Fourier propagation, an alternative approach to analyzing a diffraction problem, will reproduce the more accurate Rayleigh–Sommerfeld equation predictions. As previously noted, the Fourier components to the intensity can always be related to light path rotation and momentum exchange at the aperture.

8.1 Fresnel Zone Analysis

Opaque disc diffraction is readily described through Fresnel zone analysis. Our experimental configuration can be related to Table 1, where we define the Fresnel half zones, column B, from the edge. In Fig. 11, we count Fresnel half zones from the center of our disc. Depicted is an experimental configuration corresponding to a disc radius, $a' = R_3'$, corresponding to three Fresnel zones. The different zone lengths and corresponding effective wavelengths are the same as in Table 1. Noting the cylindrical symmetry of this configuration, the intensity pattern as a function of the radius at the screen will resemble the pattern in Fig. 3 for $X' > a'$, as we can align the x-axis with the radial axis of cylindrical coordinates for $\phi = 0$. The radial symmetry of this experiment will cause the negative deflections of light near the edge of the disc to be concentrated at the center axis of the shadow forming a Poisson's spot. The spot will vary in diameter according to the number of Fresnel half zones associated with the radius of the disc. We observed an area element at the aperture, $\rho d\rho\, d\phi$, with a light intensity, $\Phi(\rho)$, with a functional radial displacement, $f(\rho)$, has a concentrating factor ρ/R' (R' is the radial coordinate at the screen) for an area element at the screen. The deflected light intensity at R' being proportional to $\Phi'(R') = f(\rho)\Phi(\rho)\rho/R'$. This also resembles the concentrating effect

we would see for a wide electron beam deflected by a positively charged circular disc.

As in Table 1, the effective wavelength can be calculated for momentum exchange with a photon path that deflects a photon of the length of the Fresnel zone radius. Depicted in Fig. 11 is the dispersion of photon paths from a distance of $R' - R'_3$ from the edge of the disc. The solid paths are associated with a deflection of $|g| = 3/4$ and $\lambda'_e = \sqrt{6}/3$. Interior to this is the dashed path for a deflection of $|g| = 1/4$ and $\lambda'_e = \sqrt{2}$. The deflections for $g = -3/4$ converge near the central axis. We note from Fig. 8 that the same effective wavelength for deflection, $\lambda'_e = \sqrt{6}/3$, is associated with deflections from just one third of the distance to the edge, $(R' - R'_3/3)$, which is a different $g = -1/4$ deflection shown as the hashed paths closest to the edge. The net effect of a disc with a radius of three Fresnel zones is a widened spot in the center of the shadow due to the convergence of these multiple photon paths.

We note from this analysis that the relation between the effective wavelength for momentum exchange, column C, Table 1, and the deflection of a half zone, column B, when we set this equal to the radius, a'

$$\lambda'_e = \left(\frac{2}{x'_m}\right)^{\frac{1}{2}} = \frac{x'_m}{m} = \frac{a'}{m}; \qquad \lambda_e = \frac{a}{m}. \tag{53}$$

From the Fresnel zone analysis that describes the shadow profile, the odd values of m define the maxima in the intensity profile and when the center spot is observed. There are higher probabilities for momentum exchange when the effective wavelength is an odd fraction of the disc radius defined by the Fresnel number

$$\lambda_e = \frac{a}{(2j+1)} \quad \text{and} \quad Z_j \cong \frac{a^2}{(2j+1)\lambda}. \tag{54}$$

We also note from the analysis of double-slit diffraction that there may be additional higher probability momentum transfer states within the disc that focus to the axis when

$$\lambda_e = \frac{4a}{(2j+1)} \quad \text{and} \quad Z_j \cong \frac{4a^2}{(2j+1)\lambda}. \tag{55}$$

8.2 General Formalism

Sections 6–8 provided phenomenological descriptions of diffraction without invoking a wave character to the scattered photons. Here, I present the principles developed for MET in a more generalized mathematical formalism drawing upon our earlier reference to elastic Thomson scattering to integrate the role of polarization. In COW theory, the dependence on polarization is a degree of freedom for only the incident wave, whereas in MET, the polarization of the momentum exchange state and the incident light can vary independently. We have seen that COW equations, e.g., [Eq. (5)], can be related to momentum exchange probabilities dependent upon the geometries at an aperture and that this relation is implied through the properties of the Fourier transform. We replaced the concept of propagating Huygens wavelets with the deflection of photon paths connected to specific selection rules for exchange with specific momentum states of the aperture. MET moves us from defining

the probability of photon diffraction at a distant detection point to defining the probability where the photon is scattered. The critical differences from historical approaches are the assumptions of narrowly defined paths for the scattered photons and specific locations determining the momentum exchange.

In an earlier paper, I examined the question whether the larger values for g were a result of higher order momentum exchanges or multiple exchanges.[5] Multiple exchanges would align with the suggestions by Storey et al.[23] and Scully et al.[48] that the momentum kicks derive from multiple momentum exchanges with the scattered particle. Though viable, at issue with that interpretation is the necessary interaction time for multiple exchanges with a passing photon. This issue might be addressed by pulsed laser experiments.

Here, I assume the possibility of higher order momentum transfer. We have noted from Eq. (41) and Fig. 8, the geometric selection rules for momentum exchange that defines these probabilities. There are momentum exchange states at the aperture that selectively interact with the paths of passing photons resulting in quantized momentum exchange. We saw the effective wavelengths or wavenumbers for momentum exchange corresponded to those of photons with microwave energies. We know from Planck's black body radiation equation that an absorbing material body will be in thermal equilibrium, absorbing and emitting microwave frequencies. The absorber will have a broad spectrum of internal frequencies. Brillouin scattering derives from the observation that phonons of a lattice will scatter light. With the Kapitsa–Dirac effect, we observe the diffraction of particle waves by a standing electromagnetic wave.[49] Thus, our assumption of harmonic momentum states at an aperture involved in particle scattering is consistent with other observations in electrodynamics and allows for connecting mathematical descriptions.

We have noted the probability for a specific momentum transfer, $\Pr(\mathbf{k}_j)$, would contain several components. One would be the frequency or probability density of states at the aperture, $A_j(\mathbf{k}_j)$, that could exchange momentum with a resulting vector for $\mathbf{k}_j$, $\overrightarrow{\Delta p_j} = \hbar \mathbf{k}_j$. These momentum exchange states are geometric and material functions in the x, y plane of the aperture. A second is the probability of scattering at x, y at the aperture due to the interaction of the passing photon with a specific geometric function that exchanges momentum of $\mathbf{k}_j$, $B(\mathbf{k}_j)$ $(x, y, 0)$. Thus,

$$\Pr(\mathbf{k}_j) \propto A_j(\mathbf{k}_j) B(\mathbf{k}_j)(x, y, 0). \tag{56}$$

The light scattered from a volume element at $(x, y, 0)$ will be proportional to the intensity of incident light, Φ_ν, times this probability of exchange, summed over the probability density of the different $\mathbf{k}_j$ values. In our straight-edge experiment, we were able to develop the profile of $\Pr[\mathbf{g}(x \to X)]$ for positive g by curve fitting. We saw in Eqs. (40) and (47) the probability for momentum exchange at a specific point was proportional to the square of the harmonic solutions to the Schrödinger equation for particular momentum values, $\varphi(\mathbf{k}_j)$ at specific distances from the edge

$$A_j \varphi_j(\mathbf{k}_j) = A_j \sin \mathbf{k}_j \cdot \mathbf{x}; B(\mathbf{k}_j) \propto \sin^2 \mathbf{k}_j \cdot \mathbf{x} = \varphi^*_j \varphi_j. \tag{57}$$

I will continue to reference our straight-edge experimental configuration to provide clarity for our general formalism.

We have assumed that the scattering for positive and negative values of $\mathbf{k}_j$ has equal probability, suggesting that the coefficients are equal. The sine function solutions to Eq. (57) have two degrees of freedom, positive and negative values, that we connect with the sign of the momentum exchange vector, $\mathbf{k}_j$.

We can leverage the mathematical analogy to cylindrical harmonic vectors in complex space that is used in quantum mechanics to expand the degrees of freedom in our description of the momentum exchange states and scattered photons. Such harmonic functions can be used to represent momentum state functions

$$C_i \psi_i(\mathbf{p}_i) = -iC_i \exp(i\mathbf{p}_i \cdot \mathbf{r}/\hbar), \qquad (58)$$

where

$$\mathbf{p}_i \psi_i = \hbar \mathbf{k}_i \psi_i = -i\hbar \frac{d}{dr} \psi_i. \qquad (59)$$

(This formalism is referenced with caution noting that uncertainty and reduced determinism is codified in the formalism with the use of complex numbers. Hestenes[50] suggests the internal spin rotation of quantum particles is real, as indicated by the Dirac equation, concluding the formalism should be reinterpreted to reflect real spatial variables.) As our scattering is elastic, involving absorption and emission of energy at our aperture, we might diagram our momentum exchange by

$$\psi_a^-(\mathbf{p}) + \psi_\nu^- \rightarrow \psi_a^+(-\mathbf{p}) + \psi_\nu^+(+2\mathbf{p}), \qquad (60)$$

where ψ_a and ψ_ν represent states of the aperture and incident photon, respectively, and the positive and negative superscripts designate before and after momentum exchange. With our momentum exchange, $\hbar \mathbf{k}_j = 2\mathbf{p}$.

We have noted the similarity of the geometric symmetry of the BDWs[43] to the harmonic solutions of the momentum wavefunctions of an aperture—the momentum vectors of both are perpendicular to the aperture boundary. For simplification, we assume that these momentum functions resulting in exchange are always perpendicular to the boundary and the phase is the projection on the difference vector, $\mathbf{r} - \mathbf{r}_b$, between the boundary, $\mathbf{r}_b$, and the position, $\mathbf{r}$, in (or near) the plane of the aperture. The generalized momentum states that might exchange momentum are of the form

$$C_a \psi_a = -iC_a \exp i\frac{\mathbf{k}_j}{2} \cdot (\mathbf{r} - \mathbf{r}_b). \qquad (61)$$

The probability density at $\mathbf{r}$ is as follows

$$\Pr(\mathbf{k}_a) \propto C_a \left[\frac{1}{2} - \frac{1}{4}(\psi_a^4 + \psi_a^{*4}) \right]. \qquad (62)$$

I would again note that Wiseman et al.[24,25] describe an alternative general formalism for diffraction referencing the Wigner function and Bohmian mechanics. This formalism adopts a momentum representation for particle wave function

$$\tilde{\psi}(p, t) = \frac{1}{\sqrt{2\pi\hbar}} \int dr \psi(r, t) \exp \frac{i\mathbf{p} \cdot \mathbf{r}}{\hbar}. \qquad (63)$$

The perturbation of the wave function under momentum exchange is represented by

$$\tilde{\psi}_\xi(p, 0^+) = \frac{1}{\sqrt{2\pi\hbar N_\xi}} \int dp' \tilde{\psi}_0(p - p', 0^-) \tilde{O}_\xi(p'), \qquad (64)$$

where the initial momentum wave function of incident light, $\tilde{\psi}_0(p, 0^-)$, is convolved with $\tilde{O}_\xi(p')$ to give the final wave function, $\tilde{\psi}_\xi(p, 0^+)$. $\tilde{O}_\xi(p')$ is the amplitude to transfer momentum, p', giving the momentum vector result indexed by ξ. The momentum transfer function in this formalism can be correlated to the momentum exchange functions of the aperture or lattice. We might represent this connection through

$$O_\xi(x) = \sqrt{N_\xi} \exp(i\mathbf{k}_j \cdot \mathbf{x}), \qquad (65)$$

where $\mathbf{k}_j$ connects to our momentum exchange values, such as in Eqs. (14), (41), and (46).

To this point, we have neglected the effects of polarization of the scattered photon relative to the momentum exchange functions. These terms can be integrated into the cross-section here. We can connect a polarization vector, $\mathbf{E}_a$, to our momentum exchange function that is perpendicular to the vector $\mathbf{k}_\xi$. The distribution of polarizations may correspond to the distributions in our harmonic phase rotations. This may allow us to analyze the possible contribution of state polarization to the diffraction pattern, examining the functional dependence of this polarization related to that of the scattered photon, $u(\mathbf{E}_\nu \cdot \mathbf{E}_j)$. Such interactions for edge diffraction have been noted.[51] (This may be related to the requirement that the exchange function is perpendicular to the aperture boundary.) Equation (64) is modified to

$$\tilde{\psi}_\xi(p, 0^+) = \frac{1}{\sqrt{2\pi\hbar N_\xi}} \int dp' \tilde{\psi}_0(p - p', 0^-) u(\mathbf{E}_\nu \cdot \mathbf{E}_j) \tilde{O}_\xi(p'). \qquad (66)$$

9 Experimental Implications and Predictions

MET provides a simplification to the analysis of diffraction for a broadened set of experimental configurations, where the variable paths and intensity of the diffracted light must be taken into account. We find such conditions frequently with the diffraction of narrow laser beams. The approach may also simplify analysis of polygon apertures such as triangles. We can illustrate with scattering by a straight edge. Figure 7 predicts the distribution of light at the aperture point distance, x', for a narrow width of light, dx'. This condition of light scattered at such a point may be approximated by a very narrow, collimated laser beam. For such a laser beam, the theoretical predictions using Eqs. (9) and (21) based upon the Huygens–Fresnel principle, might be replaced using the experimentally generated probability for momentum exchange $\Pr[g(x' \rightarrow X')]$ in Eq. (40), associated with the specific values of g that scatter photons to X'
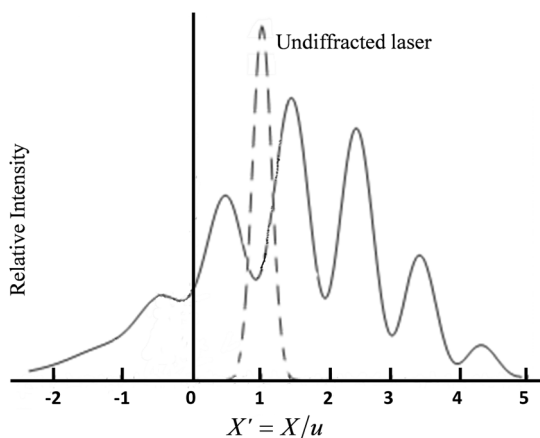
Fig. 12 Predicted plot for an experimental straight-edge diffraction pattern for a narrow, collimated Gaussian laser beam based on the probabilities for g from Fig. 7 and Eqs. (39) and (41). The laser is centered at $(x', y') = (1,0)$, with the origin at the edge and $a' = 0.2$ in Fresnel units. (Beam divergence is neglected though substantial.) The key prediction is the peak separations. The broader the laser, the less resolved these peaks will be. An obliquity factor has been estimated to diminish the intensity from the center of the beam, thus the relative heights of the different peaks are poorly estimated.

$$I(X, 0, Z) \propto \int_x \Phi(x, y, 0) \left| \frac{dx}{dX} \right| \Pr[g(x \to X)] dx$$
$$\propto \int_x \Phi(x, y, 0) \left| \frac{dx}{dX} \right| (\sin^2 2\pi g) \exp\left(\frac{-|g|}{a} \right) dx, \quad (67)$$

where $\Phi(x, y, 0)$ is the intensity at the aperture. We might set up an experiment that replicates the geometry of the apparatus in Fig. 4. Under uniform illumination of this experimental configuration, the third peak in the diffraction pattern would be found near $X_1 = 3u$, $(X_1' = 3)$. Thus, with this configuration and location of our detector at Z, we can set a laser beam centered at $x' = 1$ above our thin diffracting edge. From Eq. (27), we obtain

$$X' = x' + \frac{2g}{x'}, \qquad \Delta X' = \frac{2g}{x'}. \quad (68)$$

Thus, with a very narrow laser beam of photons at $x' = 1$, the scattering probability or intensity profile will resemble that for g in Fig. 7 except for a scaling factor of 2. The broader the beam or the greater the width of our photon detector field, the broader and more poorly resolved our peaks will be.

Figure 12 provides a predicted plot for such an experimental diffraction pattern that might be observed for a narrow Gaussian laser beam centered at (x_b', y_b') with an intensity cross-section defined by

$$\Phi(x', y') = A_b \exp \frac{-(x' - x_b')^2}{a'^2} \exp \frac{-(y' - y_b')^2}{a'^2}, \quad (69)$$

where a', the width at $1/e$, is set to equal 0.2. We note, if we enter this beam distribution in Eq. (8) replacing the uniform illumination, the equation remains separable into x and y components as in Eq. (12). The integration of the y-component for our straight-edge experiment generates a Gaussian distribution centered at y_b' and indicates our y distribution should be independent from our x distribution. Thus, the
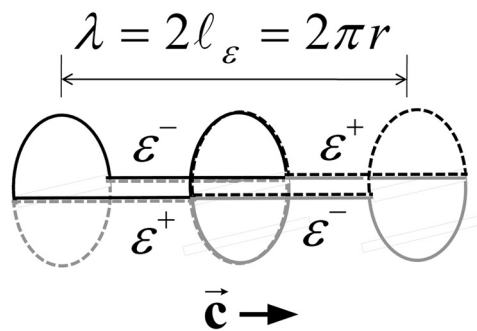
profile of Fig. 12 predicts x dependence of the diffraction profile for a series of spots centered at $Y' = y_b'$, the center of the laser beam, which can be set at $y_b' = 0$.

10 Discussion

10.1 Photon

MET relies upon a clear distinction between photon diffraction and optical interference. COW and BDW have retained broad acceptance because the wave formalism provides accurate analysis for both. A more complete picture for optics utilizing quantized and localized photons would have to explain interference and other observations that are based on phase and polarization. The success of MET in describing diffraction scattering brings further attention to the question whether a model for the photon can be developed with the necessary properties.

Several authors have suggested that the photon is geometrically extended in space.[52,53] In a recent paper, I also pointed out that the relativistic transformation of photon wavelength giving the relativistic Doppler effect provides further evidence that the wavelength is associated with a real, quantized geometric property of the photon.[54] In other words, the real geometric length of a photon is $\lambda = h/p$. In another paper, I speculated about a plausible photon model based upon four connected epsilon loops with similarity to the loops we find in string theory.[55] The rationale for that model is beyond the scope and intent of this paper. However, I reference it to suggest the feasibility of a model with more of the attributes required. This is illustrated in Fig. 13, where the four epsilon loops provide polarization, phase, and a length of λ to the photon. Two negative labeled epsilons can form an electron; two positive epsilons a positron; and a positive–negative pair a neutrino. Each epsilon contributes $h/4\lambda$ or $\hbar/4r$ to the momentum of the photon.

Fig. 13 Photon particle model. Conceptualization of a photon consisting of four connected epsilon loops that give rise to the phase, polarization, and extended length and width of the photon.[55]

10.2 Diffraction Force

QED has been a very successful theory to explain the interactions of electromagnetic particles.[29] In QED, we would describe a momentum change associated with the electromagnetic force by the transfer of a virtual photon over zero proper time and might depict this in a Feynman diagram. Photon diffraction may provide us with a very useful experimental model for the study of quantized momentum transfer and the model of virtual particles suggested by QED because photon scattering is determined by a limited set of particle momentum exchanges. Thus, diffraction experiments may

allow us to probe this phenomenon more deeply. For optical diffraction, our scattering is elastic as there is no apparent change in the wavelength and energy of the scattered photons. Thus, momentum transfer is treated as a particle scattering problem. We have described optical diffraction as involving the reflection (absorption and emission) of real or virtual photons from an edge, aperture, or lattice with additional z-momentum exchange taking place to ensure conservation of momentum and energy. This exchange might also be depicted by the exchange of two particles with momentum transfer in opposite directions.

If we can attribute a real length to a photon as in Fig. 13, then the picture of a virtual photon as a dimensionless point that arises in the vacuum of space and transitions from particle **i** to particle **j** may be misleading. If a virtual photon would have similar geometric characteristics as a real photon, then a virtual or real photon could actually bridge the gap between two interacting particles. Such a photon could form the channel between two particles that facilitates the exchange or transfer of momentum. Momentum is exchanged across this photon channel with the possibility that his channel remains intact. This virtual photon channel may provide the structure and geometry to the space between interacting particles manifesting the properties of a geometric field or vector potential. We note that the increments of momentum transfer defined in Eq. (41), $\Delta p = (2j+1)h/4x$, suggests that the material components of exchange may have a different relation of momentum to length than defined for a real photon.

Analogous to the electromagnetic field, the diffraction force may have an inverse squared dependence on distance. If neutral particles were diffracted by a dipole interaction associated with an electromagnetic field, the magnitude of the force would fall off with higher orders of power of the distance. We note that experimental observations of diffraction of starlight by the limb of the moon suggest that the formulation of the diffraction force is consistent to larger distances and, therefore, does not fall off at higher powers of distance. To provide a benchmark for this, we might refer to Fig. 4 and calculate the distances from the moon that are scattering solutions to the diffraction pattern. In a Fresnel diffraction pattern resulting from lunar occultation of starlight of 500-nm wavelength, the third maxima are observed at about 30 m from the geometric shadow.[56–58] From Eq. (28), noting the distance to the moon is 384×10^6 m, we can calculate the values for x that converge on this position of 30 m. The two approximate solutions are 15.2 and 36.6 m for $g = \pm 1.2$. These are the distances from the limb of the moon that deflect starlight to 30 m from the geometric shadow. This calculation dispels a common notion that the diffraction force is very short range (on the order of the wavelength) or must drop off extremely rapidly. Lunar occultation reinforces the premise that diffraction is determined at the location of scattering, not at distant point of detection. However, the long range of this force gives us a very broad definition for the relative location of momentum exchange. Lunar occultation also reinforces the very large magnitude of this diffraction force and the associated momentum exchanges. This observation begs the question of how the diffraction of starlight is manifested with the multiple microwave frequency exchanges that must occur in the 2 s it passes over the surface of the sun before reaching us on earth.

This diffraction force extends across a diffracting aperture and well beyond a diffracting edge, where the measurement of an electric field is negligible. Nevertheless, we see a significant influence on the diffracted particle. This suggests similarity to the Aharonov–Bohm effect, which predicts that even where the electromagnetic fields vanish, the electromagnetic potentials in the quantum domain can have significant influence.[59] This effect has been confirmed in electron diffraction experiments by double slits that are perturbed by a solenoid.[60] Could this diffraction force and the A-B effect be variations on the same quantum phenomenon? As with the A-B effect on diffracted electrons, could we observe the A-B effect on photons by modifying the electromagnetic potentials in the vicinity of our diffracting apertures?

10.3 Physics of a Connected Universe

Early observations of the wave-like properties of light led scientists to hypothesize that "luminiferous ether" permeated the universe as a medium for the propagation of light waves. The Michelson–Morley experiment and Einstein's special relativity suggested that an ether medium for the propagation of light did not exist. QED assumes the space between particles is not a vacuum, but rather consists of a quantum field teeming with "virtual" particles that constitute the medium of exchange for quantum forces. QED eliminates the issue of a preferred frame for quantum fields by the assumption that virtual particles are exchanged in proper time and exchange begins and ends at a real, material particle. Laughlin states, "The modern concept of the vacuum of space, confirmed every day by experiment, is a relativistic ether. But we do not call it this because it is taboo."[61] Dirac saw that a relativistic ether was needed to explain electrodynamics.[62] There is a renewed discussion of the role of a permeating material connecting our universe, but physicists are necessarily distinguishing this from the properties of a classical ether.[63–65] Wilczek[64] has preferred to refer to this as "the Grid." Roychoudhuri[65] has used the term a "complex tension field." Our revised description of diffraction phenomena suggests the quantum field or vector potential can replace the concept of the luminiferous ether as the origin for our observed wave-like properties. The analysis suggests that a virtual particle exchange channel could exist, establishing the field between interacting particles and potentially defining the structure of this space. This bears great similarity to the interconnectedness of particles resulting in the "implicate order," suggested by Bohm in his derivation of quantum theory.[66,67] We have already noted a relation of the defined path formalism of Bohmian mechanics to the concepts presented in MET.

11 Summary

Diffraction can be described by a statistical ensemble of particle paths determined by quantized momentum transfer related to a Fourier analysis of an aperture, where the scattering probabilities are defined at the location of scattering. Scattering probabilities are determined by at least two important factors: (1) the momentum transfer states of the scattering lattice and (2) the distance over which momentum is transferred between the lattice and scattered particle. Unique to MET is this dependence on the specific path of the scattered particle and location of momentum transfer. A detailed analysis of optical wave theory demonstrates that the underlying formalism can be connected to this quantized

momentum exchange. This has been demonstrated for a number of diffraction scenarios. Diffraction, which is treated as a particle scattering phenomenon, must be contrasted with interference, which is associated with detection when a multiplicity of photons with a correlation of their phases can mutually influence their interactions. Some optical phenomena can involve both diffraction and interference.

Diffraction can be described in terms of particle exchange using nomenclature familiar to QED. The transfer of momentum defines the diffraction force, which appears to have a universal construct linking fundamental particles, as it applies to neutral and charged particles. The manifestation of this dispersive force at the location of scattering provides an alternative to the Huygens–Fresnel principle, eliminating a critical defect in COW and its picture of Huygens wavelets by preserving conservation of momentum. This force provides a basis for quantum uncertainty that does not rely on a wave-character attributed to the scattered particle. MET assumes an integration of electromagnetic interactions at points along the photon path to derive the transfer probability that may simplify the analysis of a broadened set of aperture configurations and experimental conditions. Our analysis suggests that the associated real or virtual photons might form a channel that actually bridges the space over which the momentum is transferred. An examination of lunar occultation of starlight indicates that this diffraction force is of longer range than is generally thought for diffraction.

Acknowledgments

References

1. M. Born and E. Wolf, *Principles of Optics, Electromagnetic Theory of Propagation, Interference and Diffraction of Light*, Pergamon Press, Oxford, United Kingdom (1980).
2. M. J. Mobley, "The nature of light: a description of photon diffraction based upon virtual particle exchange," in *The Nature of Light: What Is a Photon?*, C. Roychoudhuri, K. Creath, and A. F. Kracklauer, Eds., pp. 317–332, Taylor & Francis Group LLC, Boca Raton (2008).
3. M. J. Mobley, "The nature of light: a description of photon diffraction based upon virtual particle exchange," *Proc. SPIE* **5866**, 172–182 (2005).
4. M. J. Mobley, "Diffraction described by virtual particle momentum exchange–the 'diffraction force'," *Proc. SPIE* **8121**, 81210I (2011).
5. M. J. Mobley, "Further investigation of an integrated picture of photon diffraction described by virtual particle momentum exchange," *Proc. SPIE* **8832**, 88320L (2013).
6. M. J. Mobley, "Photon diffraction described by momentum exchange theory: what more can edge diffraction tell us?" *Proc. SPIE* **9570**, 95700R (2015).
7. W. Duane, "The transfer in quanta of radiation momentum to matter," *Proc. Natl. Acad. Sci. U. S. A.* **9**, 158–164 (1923).
8. A. Landé, "Quantum fact and fiction," *Am. J. Phys.* **33**, 123–127 (1965).
9. A. Landé, "Quantum fact and fiction II," *Am. J. Phys.* **34**, 1160–1163 (1966).
10. A. Landé, "Quantum fact and fiction III," *Am. J. Phys.* **37**, 541–548 (1969).
11. A. Landé, *Quantum Mechanics in a New Key*, Exposition Press, New York (1973).
12. F. Selleri, Ed., *Wave-Particle Duality*, Plenum Press, New York (1992).
13. W. E. Lamb, Jr., "Anti-photon," *Appl. Phys. B* **60**, 77–84 (1995).
14. S. Diner et al., Eds., *The Wave-Particle Dualism: a Tribute to Louis de Broglie on his 90th Birthday*, D. Reidel Company, Dordrecht, The Netherlands (1984).
15. C. Roychoudhuri, A. F. Kracklauer, and K. Creath, Eds., *The Nature of Light: What Is a Photon*, Taylor & Francis Group, LLC, Boca Raton (2008).
16. P. Home, *Conceptual Foundations of Quantum Physics, an Overview from Modern Perspectives*, Plenum Press, New York (1997).
17. P. Ehrenfest and P. Epstein, "The quantum theory of the Fraunhofer diffraction," *Proc. Natl. Acad. Sci. U. S. A.* **10**, 133–139 (1924).
18. G. Chartier, *Introduction to Optics*, pp. 342–349, Springer Science, New York (2005).
19. J. W. Goodman, *Introduction to Fourier Optics*, pp. 37–60, McGraw-Hill, New York (1968).
20. C. M. Van Vliet, "Linear momentum quantization in periodic structures II," *Phys. A* **389**, 1585–1593 (2010).
21. L. E. Ballentine, "The statistical interpretation of quantum mechanics," *Rev. Mod. Phys.* **42**, 358–381 (1970).
22. R. P. Feynman and A. R. Hibbs, *Quantum Mechanics and Path Integrals*, McGraw-Hill, New York (1965).
23. P. Storey et al., "Path detection and the uncertainty principle," *Nature* **367**(6464), 626–628 (1994)
24. H. M. Wiseman et al., "Nonlocal momentum transfer in welcher Weg measurements," *Phys. Rev. A* **56**(1), 55–75 (1997).
25. H. M. Wiseman, "Bohmian analysis of momentum transfer in welcher Weg measurements," *Phys. Rev. A* **58**(3), 1740–1756 (1998).
26. F. S. Harris, Jr., M. S. Tavenner, and R. L. Mitchell, "Single-slit Fresnel diffraction patterns: comparison of experimental and theoretical results," *J. Opt. Soc. Am.* **59**(3), 293–297 (1969).
27. J. E. Pearson et al., "Diffraction of Gaussian laser beams by a semi-infinite plane," *J. Opt. Soc. Am.* **59**(11), 1440–1445 (1969).
28. J. M. Cowley, *Diffraction Physics*, North-Holland Publishing Co., Amsterdam, The Netherlands (1975).
29. R. P. Feynman, *Quantum Electrodynamics*, Benjamin/Cummings Publishing, Reading, Massachusetts (1983).
30. A. Sommerfeld, *Optics, Volume IV of Lectures in Lectures in Theoretical Physics*, pp. 179–272, Academic Press, New York (1954).
31. K. Miyamoto and E. Wolf, "Generalization of the Maggi-Rubinowicz, theory of boundary diffraction wave–Part I," *J. Opt. Soc. Am.* **52**, 615–625 (1962).
32. K. Miyamoto and E. Wolf, "Generalization of the Maggi-Rubinowicz theory of boundary diffraction wave–Part II," *J. Opt. Soc. Am.* **52**, 626–637 (1962).
33. J. B. Keller, "Geometrical theory of diffraction," *J. Opt. Soc. Am.* **52**, 116–130 (1962).
34. R. Kumar et al., "Knife-edge diffraction pattern as an interference phenomenon: an experimental reality," *Opt. Laser Technol.* **39**, 256–261 (2007).
35. R. Kumar, "Structure of boundary diffraction wave revisited," *Appl. Phys. B* **90**, 379–382 (2008).
36. Y. Z. Umul, "The relation between the boundary diffraction wave theory and physical optics," *Opt. Commun.* **281**, 4844–4848 (2008).
37. K. K. Sharma, *Optics: Principles and Applications*, pp. 339–458, Academic Press, Elsevier, Burlington, Massachusetts (2006).
38. O. K. Ersoy, *Diffraction Fourier Optics and Imaging*, pp. 41–83, John Wiley & Sons, Inc., Hoboken, New Jersey (2007).
39. R. G. Wilson, *Fourier Series and Optical Transform Techniques in Contemporary Optics–an Introduction*, pp. 99–129, John Wiley & Sons, Inc., New York (1995).
40. J. E. Southwell, "Validity of the Fresnel approximation in the near field," *J. Opt. Soc. Am.* **71**, 7–14 (1981).
41. A. M. Steane and H. N. Rutt, "Diffraction calculations in the near field and the validity of the Fresnel approximation," *J. Opt. Soc. Am. A* **6**(12), 1809–1814 (1989).
42. F. L. Pedrotti, L. S. Pedrotti, and L. M. Pedrotti, *Introduction to Optics*, Pearson Prentice Hall, Upper Saddle River, New Jersey (2007).
43. J. Schwinger et al., *Classical Electrodynamics*, pp. 509–520, Perseus Books, Reading, Massachusetts (1998).
44. A. Guinier, "X-ray diffraction," in *Crystals, Imperfect Crystals, and Amorphous Bodies*, W. H. Freeman and Co., New York (1963).
45. J. Wen, Y. Zhang, and M. Xiao, "The Talbot effect: recent advances in classical optics, nonlinear optics, and quantum optics," *Adv. Opt. Photonics* **5**, 83–130 (2013).
46. C. A. Bennett, *Principles of Physical Optics*, p. 319, John Wiley & Sons, Inc., Hoboken (2008).
47. R. L. Lucke, "Rayleigh-Sommerfeld diffraction and Poisson's spot," *Eur. J. Phys.* **27**, 193–204 (2006).
48. M. O. Scully, B.-G. Englert, and H. Walther, "Quantum optical tests of complementarity," *Nature* **351**, 111–116 (1991).
49. G.A. Delone et al., "The Kapitsa-Dirac resonance effect," *Opt. Commun.* **33**(2), 149–152 (1980).
50. D. Hestenes, "Zitterbewegung in quantum mechanics," *Found. Phys.* **40**, 1–54 (2010).
51. A. Y. Bekshaev, "Spin-orbit interaction of light and diffraction of polarized beams," *J. Opt.* **19**(8), 085602 (2017).
52. G. Hunter and R. L. P. Wadlinger, "Photons and neutrinos as electromagnetic solitons," *Phys. Essays* **2**(2), 158–172 (1989).
53. P. Kamenov and B. Slavov, "The photon as a soliton," *Found. Phys. Lett.* **11**, 325–342 (1998).
54. M. J. Mobley, "The relativistic transformation of wavelength provides insights into the geometry of photons," *Proc. SPIE* **7421**, 74210G (2009).

55. M. J. Mobley, "A convergence: special relativity, zitterbewegung, and new models for the subcomponent structure of quantum particles," *Proc. SPIE* **9570**, 957003 (2015).
56. M. Richmond, "Diffraction effects during a lunar occultation," http://spiff.rit.edu/richmond/occult/bessel/bessel.html (5 May 2016).
57. A. Richichi, "Model-independent retrieval of brightness profiles from lunar occultation lightcurves in near infrared domain," *Astron. Astrophys.* **226**(1), 366–372 (1989).
58. A. Richichi and A. Glindemann, "Advances in the interpretation and analysis of lunar occultation light curves," *Astron. Astrophys.* **538**, A56 (2012).
59. Y. Aharonov and D. Bohm, "Further considerations on electromagnetic potentials in the quantum theory," *Phys. Rev.* **123**, 1511–1524 (1961).
60. S. Olariu and I. I. Popescu, "The quantum effects of electromagnetic fluxes," *Rev. Mod. Phys.* **57**, 339–436 (1985).
61. R. B. Laughlin, *A Different Universe: Reinventing Physics from the Bottom Down*, pp. 120–121, Basic Books, New York (2005).
62. P. A. M. Dirac, "Is there an Aether?" *Nature* **168**, 906–907 (1951)
63. J.-P. Vigier, "Non-locality, causality and aether in quantum mechanics," *Astron. Nachr.* **303**, 55–80 (1982).
64. F. Wilczek, *The Lightness of Being: Mass, Ether, and the Unification of Forces*, pp. 73–111, Basic Books, New York (2010).
65. C. Roychoudhuri, "The constancy of 'c' everywhere requires the cosmic space to be a stationary and complex tension field," *Proc. SPIE* **8121**, 81210P (2011).
66. D. Bohm, *Wholeness and Implicate Order*, Routledge and Kegan Paul, London, United Kingdom (1980).
67. D. Bohm and B. J. Hiley, *The Undivided Universe*, Routledge, London, United Kingdom (1993).

Michael J. Mobley is a professor in the College of Science, Engineering, and Technology at Grand Canyon University, former associate director at the Biodesign Institute at Arizona State University, and former director of R&D at the Procter & Gamble Company. He received his MS degree in chemical physics from Simon Fraser University and his PhD in physical chemistry from Arizona State University. He is the author in more than 20 journal publications and holds four patents. His research expertise is in molecular spectroscopy, chemical physics, optics, biomedical diagnostics, and theoretical physics.